Title
ANALYSIS OF PION HELIUM SCATTERING FOR THE PION CHARGE FORM FACTOR

Author
Mottershead, C.T.

Publication Date
1969-06-01

Submitted to Physical Review;
Also submitted as a Ph. D. Thesis

UCRL-19216
Preprint

c.2

ANALYSIS OF PION HELIUM SCATTERING FOR THE PION CHARGE FORM FACTOR

C. T. Mottershead

June 10, 1969

AEC Contract No. W-7405-eng-48

LAWRENCE RADIATION LABORATORY
UNIVERSITY of CALIFORNIA BERKELEY

DISCLAIMER

Contents

UCRL-19216

ANALYSIS OF PION HELIUM SCATTERING FOR THE PION CHARGE FORM FACTOR*

C. T. Mottershead

Lawrence Radiation Laboratory
University of California
Berkeley, California

June 10, 1969

ABSTRACT

Elastic scattering of π^+ and π^- on He^4 is analysed for information on the charge radius of the pion using a new method based on boundary conditions near the nuclear surface. The pion radius enters the calculation via the electrostatic potential of the pion and Helium charge distributions, which is assumed to be the only charge dependent interaction. Since He^4 is isoscalar the strong nuclear interaction is assumed charge independent. Differential cross section data for both signs of the charge are fit simultaneously by a program that uses the logarithmic derivatives of the pion radial wave function for each charge as free parameters. If the nuclear interaction operator is symmetric (i.e. $\langle \underset{\sim}{r}' | U_N | \underset{\sim}{r} \rangle = \langle \underset{\sim}{r} | U_N | \underset{\sim}{r}' \rangle$), the difference in the logarithmic derivative for a given partial wave due to changing the sign of the charge may be expressed as an integral of the internal Coulomb potential weighted by the wave function. Nuclear model dependence is greatly reduced by the constraints imposed by the empirical boundary conditions on the internal wave function. The Crowe Group's data at beam momenta of 130 to 163 MeV/c are analysed by this method using both local potential and Kisslinger models for the strong interaction, and Gaussian and Yukawa pion charge distributions. The results indicate $2.2 < r_\pi < 3.2$ F, depending on theoretical model, with an experimental

precision of $\sim \pm 0.5$ F . In the course of the analysis, the singular point difficulty with the Kisslinger model was examined and found to be serious. A simple treatment of the relativistic reduced mass (two body problem) is given in an appendix.

I. INTRODUCTION

The possibility of measuring the pion electromagnetic form factor by comparing the elastic scattering of π^+ and π^- beams on an isoscalar target nucleus such as He^4 has been the subject of a series of recent papers.[1-9] The key assumption of these studies is that the strong nuclear interaction, whatever its detailed nature, is the same for both pion charges, while the Coulomb potential is the same except for sign. This Coulomb potential, which is taken to be the only electromagnetic interaction, depends on the charge distributions of the pion and nucleus, and thus on the parameters of their respective form factors. The general plan is to analyse the differential cross section data for both charges to separate the nuclear and Coulomb contributions to the scattering amplitude. If the nuclear charge distribution is known, the Coulomb contribution may then be interpreted as a measurement of the pion charge radius.

Accurate calculations, with the fewest possible approximations, are needed to find the small effects due to pion size in the large nuclear scattering amplitudes. It is also essential to reduce the effect of the uncertainties in the pion-nucleus interaction by using model independent methods as far as possible. With these objectives, two methods of analysis have so far been proposed:

(i) Optical model analysis. The emphasis here is on calculational accuracy.[1-3] The nuclear interaction is represented by an optical model potential and the Schrödinger equation integrated numerically for both signs of the charge. The parameters of both the optical and Coulomb potentials are then adjusted to fit the cross section data. An exact solution is obtained for the given model, but the method mixes the

Coulomb and nuclear parts of the problem, so the pion radius obtained may depend on the model chosen.

(ii) Coulomb perturbation methods. These emphasize model independence.[5-9] The nuclear amplitude is parameterized by a set of phase shifts, and the Coulomb Born amplitude, which is proportional to the product of the form factors, is explicitly separated out. The method is less model dependent than (i), and it avoids the use of Coulomb wave functions, but it introduces an important first order Coulomb-nuclear interference ("distortion") amplitude that is given by a logarithmically divergent integral.

A third method of analysis, using the same basic assumptions as the above two, is proposed in Sec. II of this paper in an effort to combine calculational accuracy with model independence. A close fitting boundary surface (radius R) is drawn around the nucleus, and the Coulomb potential $\pm Ze^2/r$ is assumed to be the only interaction in the external region $(r \geq R)$. As in (i), the exact external solution of the Schrödinger equation is expressed in terms of Coulomb wave functions, and related to the logarithmic derivative of the interior solution at the boundary. These logarithmic derivatives, however, are taken as free parameters, thus giving a model independent fit to the cross section data, while avoiding the divergence difficulties that arise in perturbation treatments of the long range part of the Coulomb potential. The interior Coulomb perturbation on the logarithmic derivatives is then derived for a very general form of nuclear interaction operator, and turns out to be only slightly model dependent.

In Sec. III the method is applied to the Crowe Group's data to

determine the empirical boundary conditions at $r = R$. The relevant aspects of models for the pion-nucleus interaction are discussed in Sec. IV, and the conclusions about the pion size given in Sec. V. Finally, the effects of some alternative assumptions are discussed in Sec. VI.

II. THE BOUNDARY CONDITION METHOD

The Klein Gordon equation for the motion of a pion of energy E_π and charge te ($t = +1, 0,$ or -1) in a fixed electrostatic potential Ze/r may be written

$$\left[\nabla^2 + k^2 - t\cdot 2\eta k/r\right]\psi^t(\underset{\sim}{r}) = 0 \quad , \tag{1}$$

where $k = \left(E_\pi^2 - m_\pi^2\right)^{\frac{1}{2}}$ is the asymptotic momentum of the pion, and $\eta = Ze^2/\beta$ is the Coulomb scattering strength parameter for velocity $\beta = k/E_\pi$. A second order term in the potential, which is less than $10^{-4}k^2$ for our pion-Helium scattering problem, has been omitted from Eq. (1) so that conventional Coulomb functions may be used in its solution. We slightly generalize Eq. (1) by taking k to be the momentum and β the relative velocity in the center of mass coordinate system as computed according to conventional two body relativistic kinematics. Then $\psi^t(\underset{\sim}{r})$ is interpreted as the probability amplitude for the interparticle separation $\underset{\sim}{r}$. A simple rationalization of this compromise to allow for both nuclear recoil motion and relativistic kinematics is given in appendix A. In any case, we assume Eq. (1) applies to the pion-nucleus system when the pion is outside some small sphere of radius R centered on the nucleus.

On substitution of the partial wave expansion

$$\psi^t(\underset{\sim}{r}) = \frac{1}{kr}\sum_{\ell=0}^{\infty}(2\ell + 1)\, i^\ell\, u_\ell^t(r)\, P_\ell(\cos\theta) \tag{2}$$

into Eq. (1), we find that the radial wave function $u_\ell^t(r)$ satisfies the Coulomb radial equation

$$\left\{\frac{d^2}{dr^2} - \frac{\ell(\ell+1)}{r^2} + k^2 - \frac{2t\eta k}{r}\right\} u_\ell^t(r) = 0 \quad . \tag{3}$$

It therefore must be of the form (for $r > R$)

$$u_\ell^t(r) = A_\ell^t \left[\cos \delta_\ell^t F_\ell(t\eta, kr) + \sin \delta_\ell^t G_\ell(t\eta, kr)\right] . \tag{4}$$

Where $F_\ell(\eta, x)$ and $G_\ell(\eta, x)$ are the standard regular and irregular Coulomb functions, and $(A_\ell^t, \delta_\ell^t)$ are constants to be determined. The asymptotic form of Eq. (4) is

$$u_\ell^t(r) \underset{r\to\infty}{\sim} A_\ell \sin\left(kr - t\eta\, \ell n(2kr) - \frac{\ell\pi}{2} + \sigma_\ell(t\eta) + \delta_\ell^t\right) . \tag{5}$$

Here $\sigma_\ell(\eta) \equiv \arg \Gamma(\ell + 1 + i\eta)$ is the conventional Coulomb phase shift, and δ_ℓ^t is interpreted as an additional phase shift due to whatever deviations there are (for $r < R$) from a pure $1/r$ potential. By consideration of its asymptotic incident and outgoing radial fluxes, this solution is shown in standard quantum mechanics texts (e.g. Ref. 10) to imply a differential cross section for elastic scattering that may be written

$$\sigma_t(\theta) = \left|f_N^t + f_c^t\right|^2 \quad . \tag{6}$$

Except for an unobservable phase, f_c^t is the usual Coulomb scattering amplitude:

$$f_c^t(q) \equiv - \frac{2t\eta k}{q^2} \exp\left[- it\eta \ln\left(\frac{q^2}{4k^2}\right)\right] . \qquad (7)$$

The momentum transfer q is related to the center of mass scattering angle θ by

$$q^2 = 2k^2(1 - \cos\theta) . \qquad (8)$$

The nuclear scattering amplitude f_N^t has the expansion

$$f_N^t(\theta) = \sum_{\ell=0}^{\infty} (2\ell + 1)\, \gamma_\ell(t\eta)\, a_\ell^t(k)\, P_\ell(\cos\theta) , \qquad (9)$$

with the nuclear partial wave amplitudes given by

$$a_\ell^t(k) \equiv \exp(2i\delta_\ell^t(k)) - 1)/2ik = \left(k \cot\delta_\ell^t - ik\right)^{-1} . \qquad (10)$$

The Coulomb phase factors

$$\gamma_\ell(\eta) \equiv \exp\ 2i(\sigma_\ell(\eta) - \sigma_0(\eta)) , \qquad (11)$$

may be conveniently generated from the recursion formulas

$$\gamma_0(\eta) = 1 ; \ \gamma_\ell(\eta) = \frac{(\ell + i\eta)^2}{(\ell^2 + \eta^2)}\, \gamma_{\ell-1}(\eta) ; \ \gamma_\ell(-\eta) = \gamma_\ell^*(\eta) . \qquad (12)$$

If Eq. (1) were valid for all r, then only the regular solution $F_\ell(\eta, x)$ would be permitted in Eq. (4), and all the δ_ℓ^t would have to be zero. Eq. (6) would then reduce to the well known Rutherford formula for pure Coulomb scattering.

Of course Eq. (1) is not valid for all r. At small distances the electrostatic potential will deviate from the 1/r form due to overlap of the charge distributions of the pion and nucleus. The pion's charge form factor is related to its charge distribution $te\rho_\pi(r)$ by

$$F_\pi(q) = \int d^3\underset{\sim}{r}\, e^{-i\underset{\sim}{q}\cdot\underset{\sim}{r}}\, \rho_\pi(r) \quad , \tag{13}$$

where $\rho_\pi(r)$ is normalized so that $F_\pi(0) = \int d^3r\, \rho_\pi(r) = 1$. Expansion of Eq. (13) in powers of q yields

$$F(q) = 1 - \frac{1}{3!}\, q^2 \langle r^2\rangle + \frac{1}{5!}\, q^4 \langle r^4\rangle - \frac{1}{7!}\, q^6 \langle r^6\rangle - \cdots \tag{14a}$$

where

$$\langle r^n\rangle \equiv \int_0^\infty r^n\, \rho(r)\, 4\pi r^2 dr \quad , \tag{14b}$$

is the nth moment of the charge distribution. The object of this paper is to develop a method for the extraction of the r.m.s. pion charge radius $r_\pi \equiv \langle r^2\rangle^{\frac{1}{2}}$ from pion nucleus scattering data. To carry out the analysis, the nuclear charge form factor $F_N(q)$, defined as in Eq. (13), must be known.

The electrostatic potential energy of two charge distributions is given in terms of their form factors $F_{\pi,\,N}(q)$ and the separation r of their centers by $V_C(r) \equiv tZe^2 v(r)$ with

$$v(r) = \frac{1}{(2\pi)^3} \int d^3q\; e^{i\underset{\sim}{q}\cdot\underset{\sim}{r}}\, F_\pi(\underset{\sim}{q})\, \frac{4\pi}{q^2}\, F_N(-\underset{\sim}{q}) = \frac{2}{\pi} \int_0^\infty \frac{\sin qr}{qr}\, F_\pi(q)\, F_N(q) dq \; . \tag{15}$$

It is sometimes more convenient to evaluate $v(r)$ by solution of Laplace's equation with an effective charge distribution $g(r)$ obtained by applying ∇^2 to both sides of Eq.(15):

$$\nabla^2 v(r) = \frac{1}{r} \frac{d^2}{dr^2} rv(r) = -4\pi g(r) , \tag{16a}$$

$$g(r) \equiv \frac{1}{(2\pi)^3} \int d^3q \; F_\pi(\underset{\sim}{q}) \, F_N(-\underset{\sim}{q}) \; e^{i\underset{\sim}{q}\cdot\underset{\sim}{r}} . \tag{16b}$$

At large distances $v(r) = 1/r$. The pion radius therefore enters the calculation only via its influence on the short range shape of $v(r)$.

As indicated by electron scattering experiments,[11] we take the He^4 nucleus to be a Gaussian shape

$$\rho_N(r) = \frac{e^{-r^2/a^2}}{\pi^{3/2} a^3} , \tag{17a}$$

with r.m.s. radius $r_N = \sqrt{\frac{3}{2}}\, a = 1.65 \pm .03$ F and form factor

$$F_N(q) = \exp\left(-\frac{q^2 r_N^2}{6}\right) . \tag{17b}$$

If the pion is also assumed to have a Gaussian shape of r.m.s. radius r_π, then the effective charge distribution is $g_G(r) = \exp(-r^2/c^2)/\pi^{3/2}c^3$, with $c^2 = \frac{2}{3}(r_N^2 + r_\pi^2)$.

The corresponding potential is

$$v_G(r) = \frac{1}{r} \operatorname{erf}\left(\frac{r}{c}\right) \quad . \tag{18}$$

An alternative pion form factor favored for dispersion relation calculations is

$$F_\pi(q) = \frac{\mu^2}{q^2 + \mu^2} \quad , \tag{19a}$$

which yields a Yukawa charge distribution

$$\rho_\pi(r) = \frac{\mu^2}{4\pi} \cdot \frac{e^{-\mu r}}{r} \quad , \tag{19b}$$

with $r_\pi = \sqrt{6}/\mu$. According to the vector dominance model, μ should be the mass of the ρ meson, leading to a predicted pion radius of $r_\pi = 0.63$ F. The corresponding potential is[14]

$$v(r) = \frac{1}{r}\left\{\operatorname{erf}\left(\frac{r}{a}\right) + \frac{1}{2}\, e^{(r_N/r_\pi)^2}\left[e^{\mu r} \operatorname{erfc}\left(\frac{r_N}{r_\pi} + \frac{r}{a}\right) - e^{-\mu r} \operatorname{erfc}\left(\frac{r_N}{r_\pi} - \frac{r}{a}\right)\right]\right\} \quad . \tag{20}$$

For $r_\pi = 0$, Eqs. (18) and (20) give identical results. Fig. 1 shows the He^4 density distribution, and the effective Coulomb potentials $V_c(r) = Ze^2 v_G(r)$ calculated from Eq. (18) for $r_\pi = 0,1,2$, and 3F. The potential for $r_\pi = 2$F according to Eq. (20), and for a point charge ($V_c = Ze^2/r$) are also shown for comparison. Beyond R = 3.5F, which we choose as the boundary radius, we have essentially $\rho_N(r) = 0$ and $v(r) = 1/r$.

In addition to this Coulomb potential, the pion for $r < R$ feels a strong nuclear interaction which we will assume to be short ranged, rotationally invariant, and charge independent. We therefore generalize Eq. (1) in the form

$$\left\{\nabla^2 + k^2 - 2t\eta kv(r)\right\} \psi^t(\underline{r}) = \int d^3\underline{r}' \langle \underline{r}|U_N|\underline{r}'\rangle \psi^t(\underline{r}') \quad , \qquad (21)$$

where $\langle \underline{r}|U_N|\underline{r}'\rangle$ is the coordinate representation of some nuclear interaction operator U_N. Charge independence means that U_N is the same for all values of the charge index t. We choose the boundary radius R so that in the external region $r \geq R$, U_N is negligible ($\langle \underline{r}|U_N|r'\rangle \cong 0$), and $v(r)$ takes its asymptotic form $1/r$, so Eq. (21) takes the form Eq. (1).

The assumption of rotational invariance means we can solve Eq. (21) one partial wave at a time. In a solution of the form

$$\psi^t(\underline{r}) = \chi_\ell{}^t(r)\, Y_\ell{}^m(\theta,\psi) \quad , \qquad (22)$$

the radial wave function χ_ℓ is determined to within a normalization constant by Eq. (21), and so its logarithmic derivative at the boundary $r = R$, defined by

$$\lambda_\ell{}^t \equiv R \left\{\frac{\partial}{\partial r} \ell n(r\chi_\ell{}^t(r)\right\}_{r=R} \quad , \qquad (23)$$

is completely determined. Since in the external region $(r \geq R)$, $\chi_\ell{}^t(r)$ must take the form $r^{-1}u_\ell{}^t(r)$, with $u_\ell{}^t(r)$ given by Eq. (4), $\lambda_\ell{}^t$ is related to the nuclear phase shift $\delta_\ell{}^t$ by

$$\lambda_\ell^{\,t} = \left\{ \frac{xG_\ell'(t\eta, x) + \cot\delta_\ell^{\,t} \cdot x F_\ell'(t\eta, x)}{G_\ell(t\eta, x) + \cot\delta_\ell^{\,t} \cdot F_\ell(t\eta, x)} \right\}_{x=kR} , \quad (24)$$

where $F_\ell'(\eta, x) \equiv \frac{\partial F_\ell(\eta, x)}{\partial x}$ ··· etc.

For the experiment in question (130-160 MeV/c $\pi^\pm$ on He^4), the whole Coulomb potential $V_c(r)$ inside $r = R$ is a small perturbation on the energy and strong interaction terms in Eq. (21). Therefore changing the sign of V_c should induce only a small shift in $\lambda_\ell^{\,t}$. Writing

$$\lambda_\ell^{\pm}(k, R) \equiv S_\ell(k, R) \pm \eta D_\ell(k, R) , \quad (25)$$

we expect the average logarithmic derivative $S_\ell = \frac{1}{2}(\lambda_\ell^{+} + \lambda_\ell^{-})$ to depend mainly on the strong interaction, while the difference $D_\ell = (\lambda_\ell^{+} - \lambda_\ell^{-})/2\eta$ should depend mainly on the Coulomb effects. From Eqs. (10, 24, and 25) we obtain

$$a_\ell^{\pm} = -\frac{1}{k} \left\{ \frac{(S_\ell \pm \eta D_\ell) F_\ell(\pm\eta, x) - x F_\ell'(\pm\eta, x)}{(S_\ell \pm \eta D_\ell) H_\ell(\pm\eta, x) - x H_\ell'(\pm\eta, x)} \right\}_{x=kR} , \quad (26)$$

where

$$H_\ell(\eta, x) \equiv G_\ell(\eta, x) + i F_\ell(\eta, x) .$$

Thus, when Eq. (1) applies in the external region ($r \geq R$), the variables (S_ℓ, D_ℓ) give a parameterization of the observable nuclear partial wave amplitudes $a_\ell^{\pm}$ as general as phase shift analysis, but with the added advantage (important in practice) that data for both signs of the charge may be fit simultaneously.

For large ℓ, where the phase shifts δ_ℓ^t are zero, λ_ℓ^t is just the logarithmic derivative of the regular Coulomb function $F_\ell(t\eta, kr)$. Only the first few nuclear partial waves are expected to be nonzero, and so all the information available in the experiment about both the nuclear interaction and the pion radius must be contained in the corresponding values of S_ℓ and D_ℓ. A computer program was written, using the Berkeley χ^2 minimization routine VARMIT, that adjusts S_ℓ and D_ℓ for the first few partial waves to fit the $\pi^\pm He^4$ scattering data. The result of its application to the Crowe Group data at 130 to 163 MeV/c will be discussed in Sec. III of this paper. For the remainder of Sec. II, S_ℓ and D_ℓ should be viewed as empirical quantities summarizing the data.

Formulas for the interpretation of the fit parameters (S_ℓ, D_ℓ) in terms of $v(r)$ and the internal radial wave function may be derived as follows: Multiply Eq. (21) by the wave function for charge index t', subtract the corresponding equation with t and t' interchanged, and integrate over the internal volume $|\underset{\sim}{r}| \leq R$ to obtain

$$\int_{|\underset{\sim}{r}|\leq R} d^3r \left\{\psi^{t'}(r)\,\nabla^2\psi^t(r) - \psi^t(r)\nabla^2\psi^{t'}(r) + 2\eta k(t' - t)v(r)\psi^{t'}(r)\psi^t(r)\right\} =$$

$$\int_{|\underset{\sim}{r}|\leq R} d^3r \int d^3r' \left\{\psi^{t'}(\underset{\sim}{r})\,\langle \underset{\sim}{r}|U_N|\underset{\sim}{r}'\rangle\psi^t(\underset{\sim}{r}') - \psi^t(\underset{\sim}{r})\,\langle \underset{\sim}{r}|U_N|\underset{\sim}{r}'\rangle\psi^{t'}(\underset{\sim}{r}')\right\} . \tag{27}$$

The integral on d^3r on the right side of Eq. (27) may be extended over all space, since by assumption $\langle r|U_N|r'\rangle = 0$ for $|\underset{\sim}{r}| > R$. If we now further assume that the nuclear interaction operator is symmetric,

$$\langle \underset{\sim}{r}'|U_N|\underset{\sim}{r}\rangle = \langle \underset{\sim}{r}|U_N|\underset{\sim}{r}'\rangle \quad , \tag{28}$$

then the entire right side vanishes, since r and r' are equivalent dummy integration variables and may be interchanged in the first integrand. Local potentials ($\langle \underset{\sim}{r}'|U_N|\underset{\sim}{r}\rangle = U_N(\underset{\sim}{r})\,\delta(\underset{\sim}{r}-\underset{\sim}{r}')$) are certainly symmetric, as are a wide class of optical potentials derived from multiple scattering theory (see Sec. IV for proof), so Eq. (28) is not unduly restrictive. Using vector identities and Gauss' law, Eq. (27) may be transformed into

$$R^2 \oint d\Omega \left[\psi^{t'} \frac{\partial \psi^{t}}{\partial r} - \psi^{t} \frac{\partial \psi^{t'}}{\partial r} \right]_{r=R} = 2\eta k(t-t') \times \oint d\Omega \int_0^R r^2\, v(r) \psi^{t'}(r) \psi^{t}(r)\, dr \quad . \tag{29}$$

The angular integration may be done using Eq. (22) and the orthonormality of the spherical harmonics. Then, assuming R is chosen so that $\chi_\ell^{\,t}(R) \neq 0$, divide through by $R\chi_\ell^{\,t'}(R)\chi_\ell^{\,t}(R)$ and use Eq. (23) to obtain

$$\lambda_\ell^{\,t} - \lambda_\ell^{\,t'} = 2\eta k R(t-t') \int_0^R v(r) y_\ell^{\,t'}(r) y_\ell^{\,t}(r)\, dr, \tag{30}$$

where $y_\ell^{\,t}(r) \equiv r\chi_\ell^{\,t}(r)/R\chi_\ell^{\,t}(R)$ is the radial wave function normalized to unity at the upper limit $r=R$.

Finally, taking $t' = 0$, $t = \pm 1$, we derive the following exact formulas for S_ℓ and D_ℓ:

$$S_\ell = \lambda_\ell^{\,0} + \eta kR \int_0^R v(r)\, y_\ell^{\,0}(r) \left[y_\ell^{\,+}(r) - y_\ell^{\,-}(r) \right] dr \quad , \tag{31}$$

$$D_\ell = 2kR \int_0^R v(r)\; y_\ell^{\,0}(r) \cdot \frac{1}{2}\left[y_\ell^{\,+}(r) + y_\ell^{\,-}(r)\; dr \right] \quad . \tag{32}$$

All the wave functions behave near the origin as $y_\ell^{\,t}(r) \cong$ const. $\times\, r^{\ell+1}$ and are by definition equal at the upper limit: $y_\ell^{\,+}(R) = y_\ell^{\,-}(R) = y_\ell^{\,0}(R) = 1$. The effect of the Coulomb potential is to give $y_\ell^{\,-}(r)$ slightly more curvature than $y_\ell^{\,0}(r)$, and $y_\ell^{\,+}(r)$ slightly less. Therefore it should be a good approximation in Eq. (32) to put

$$\frac{1}{2}\left(y_\ell^{\,+}(r) + y_\ell^{\,-}(r)\right) \cong y_\ell^{\,0}(r) \quad . \tag{33}$$

Also, since the difference $y_\ell^{\,t}(r) - y_\ell^{\,-}(r)$ vanishes at both limits and is expected generally to be of order η, the second term in Eq. (31) is of order $\eta^2 = .0004$ and is negligible. We may therefore interpret the fit parameters S_ℓ, D_ℓ by the working approximations

$$S_\ell \cong \lambda_\ell^{\,0} = R \left[\frac{\partial}{\partial r}\; \ell n\left(r \chi_\ell^{\,0}(r)\right) \right]_{r=R} = R \left. \frac{dy_\ell^{\,0}(r)}{dr} \right|_{r=R} \quad . \tag{34}$$

$$D_\ell \cong 2kR \int_0^R v(r) \left[y_\ell^0(r) \right]^2 dr \quad . \qquad (35)$$

For the best fitting nuclear models of Sec. IV, the error in these approximations is $\lesssim 0.2\%$ for Eq. (34), and $\lesssim 0.1\%$ for Eq. (35). Since this is well within the experimental uncertainties (Table I), Eqs. (34) and (35) are entirely adequate for our present purposes.

The role of the nuclear interaction model in the analysis is now clear: it is to provide a reasonable internal wave function so that the observed value of D_ℓ may be interpreted according to Eq. (35) in terms of the effective Coulomb potential. The parameters of the model are to be adjusted so the logarithmic derivative of the neutral ($t = 0$) wave function satisfies Eq. (34) for the observed values of S_ℓ. But no matter what model is used, the weighting function $\left(y_\ell^0(r)\right)^2$ must always satisfy:

$$y_\ell^{0^2}(r) \cong \text{const} \cdot r^{2\ell+2} \quad \text{for small } r, \qquad (36a)$$

$$\left[y_\ell^{0^2} \right]_{r=R} = 1 \quad , \quad \text{and} \quad \left\{ \frac{d}{dr} \left(y_\ell^{0^2} \right) \right\}_{r=R} = \frac{2S_\ell}{R} \quad . \qquad (36b)$$

These constraints on the form of y_ℓ serve in practice to greatly reduce the sensitivity of D_ℓ to the details of the nuclear interaction. The boundary condition method outlined above thus provides a good separation between the strong and electrodynamic parts of the problem.

The general behavior of S_ℓ and D_ℓ may be anticipated from Eqs. (34) and (35). The pion radius determines essentially the central value $v(0)$ of the Coulomb potential: the more diffuse the charge distribution, the shallower the potential (Fig. 1). Hence D_ℓ is a monotonically decreasing function of r_π. To increase the sensitivity of D_ℓ to r_π, the boundary radius R should be chosen as small as possible consistent with the condition $v(r) \cong 1/r$ for $r > R$. As ℓ increases, the integral in Eq. (35) is more dominated by the outermost values of $v(r)$, so D_ℓ becomes both smaller and much less sensitive to r_π. It also becomes harder to measure, since S_ℓ generally increases with ℓ, eventually taking the form $S_\ell \sim \ell + 1$, and completely dominating the D_ℓ term in Eq. (25). It is therefore the fit parameters (S_ℓ, D_ℓ) for the low partial waves, especially the S wave, that must be well determined to permit measurement of r_π. The higher partial waves need only be consistent with the general formalism.

III. DATA ANALYSIS

The Crowe group data consists of measurements of the $\pi^{\pm}$He elastic scattering differential cross sections $\sigma^{\pm}(\theta)$ at 15 scattering angles and 4 beam momenta: 130.2, 142.3, 153.2, and 163.0 MeV/c. The cross sections show a deep interference minimum of about 0.3 - 0.5 mb/sr near 70°, then rise to some 5 to 7 mb/sr in the backward direction. (Fig. 3) See their paper for the full data set and details of the experiment.[3]

From this data the fractional difference

$$\Delta(\theta) \equiv \left[\sigma^{-}(\theta) - \sigma^{+}(\theta)\right] \Big/ \left[\frac{1}{2}\left(\sigma^{-}(\theta) + \sigma^{+}(\theta)\right)\right] \qquad (37)$$

is formed. This difference is due in general to Coulomb-nuclear interference effects, and is expected to be sensitive to the pion radius, especially near the minimum where the nuclear amplitude is small and momentum transfer is not ($q \sim 0.8$ Fm^{-1}). Although $\Delta(\theta)$ is not independent information, its precision benefits from the cancellation of some uncertainties in beam normalization. The total data set thus consists of 120 cross section points $\sigma^{\pm}_{k}(\theta_i)$ and 60 semidependent derived quantities $\Delta_k(\theta_i)$.

The data was analysed independently at each beam energy using Eqs. (6 - 12), and (26). To account for inelastic processes, complex values of S_ℓ and D_ℓ were allowed in the first three partial waves ($\ell \leq 2$). Higher partial waves were omitted ($a_\ell^{\pm} \equiv 0$ for $\ell > 2$). The basic fitting procedure was to fix the D_ℓ and adjust the S_ℓ to fit the 30 cross section points ($\sigma^{\pm}(\theta_i)$ i = 1, 15) by minimizing $\chi^2_+ + \chi^2_-$ where

$$\chi_t^2 = \sum_{i=1}^{15} \left(\frac{\sigma_{calc}{}^t(\theta_i) - \sigma_{data}{}^t(\theta_i)}{\delta\sigma(\theta_i)} \right)^2 , \qquad (38)$$

and $\delta\sigma(\theta_i)$ is the experimental error. Similiarly for fixed S_ℓ, the D_ℓ were adjusted to fit the 15 $\Delta(\theta_i)$ data points by minimizing the corresponding χ_Δ^2. With the improved D_ℓ, the S_ℓ were refitted and vice versa for as many iterations as needed until the process converged.

It was found that not all of the 12 parameters (real and imaginary parts of S_ℓ and D_ℓ for $\ell = 0,1,2$) could be determined by the data. In particular, the imaginary parts were poorly constrained, since only elastic scattering data was used. Therefore only $\mathrm{Im}S_o$ and $\mathrm{Im}D_o$ were left free to fit the data, while the other imaginary parts were fixed at reasonable values. The choice of the "reasonable values" was guided by considerations of smooth energy dependence, unitarity (i.e. $\mathrm{Im}\,\delta_\ell^{\pm} \geq 0$), and, in the later stages, Eq. (35) for D_ℓ with fitted optical model wave functions. The necessity of making some such arbitrary choices is easily seen if only the main S and P wave amplitudes are considered, and the small Coulomb and D wave amplitudes neglected. In that case there would be 4 free parameters (say $\mathrm{Re}\,\delta_\ell$ and $\mathrm{Im}\,\delta_\ell$ for $\ell = 0,1$) but, since the cross section would be quadratic in $\cos\theta$, only 3 coefficients could be determined by the elastic scattering data. Although our actual case isn't so simple since we do have some sensitivity to the imaginary parts via interference with the Coulomb amplitude, the net empirical result is essentially that the combination $\mathrm{Im}\lambda_o + \text{const} \times \mathrm{Im}\lambda_1$ (const. $\approx$ 1.5) is well

determined, while the orthogonal combination $\mathrm{Im}\lambda_0 - \mathrm{Im}\lambda_1$ / const. is undetermined by the data. As a check on the imaginary parts, the absorbtion cross section was calculated from

$$\sigma_{abs}^{\pm}(k) = \frac{1}{k^2} \sum_{\ell=0}^{\infty} (2\ell + 1) \left[1 - \left| e^{2i\delta_\ell^{\pm}} \right|^2 \right] , \qquad (39)$$

and compared with the experimental values of Block et al. (Fig.2). The fair agreement lends confidence to the choices made. In any case it is the real parts that are significant for the measurement of the pion radius, and their best fitting values were essentially independent of the values chosen for the imaginary parts. The only constraint placed on the real parts was that in the final fit, $\mathrm{Re}D_2$ for 153.2 MeV/c was fixed on a smooth curve passing through the best fitting values of $\mathrm{Re}D_2$ for the other energies. This was the only constraint necessary to give a smooth energy dependence to all the fit parameters.

Table I lists the final fit parameters (S_ℓ, D_ℓ) at a boundary radius of $R = 3.5F$. The corresponding phase shifts are calculated from Eqs. (24)and(25). Table II lists some kinematic quantities, the final $\chi's^2$ achieved, and some indications of the relative accuracy of the four data sets. At each energy, the data was taken with all the cross section points having roughly the same percentage experimental error $p_i \equiv \delta\sigma(\theta_i) / \sigma(\theta_i)$, so that the fractional difference data points would have roughly equal errors $\delta\Delta(\theta_i)$. The inverse r.m.s. percentage error $\bar{p}$, defined by

$$\frac{1}{\bar{p}^2} \equiv \frac{1}{N} \sum_{i=1}^{N} \frac{1}{p_i^2} , \qquad (40)$$

is given as a measure of the precision of the cross section data. The inverse r.m.s. error $\overline{\delta\Delta}$, defined similarly, specifies the average weight of the $\Delta(\theta_i)$ data points (cf. Eq. 38), and hence the scale of the corresponding χ_Δ. It should be noted that although the 142.3 MeV/c data has the highest χ's^2, it also has the greatest statistical precision, and in fact yields the best fits relative to the scale of its χ^2. This is also apparent in Figs. 3 and 4, where the best fit curves calculated from Eqs. (6-12), (25), (26), and (37), using the values of S_ℓ and D_ℓ in Table I, are shown with the data points. It should be emphasized at this point that, except for the assumption that Eq. (1) applies for $r>R$, the values given in Table I are a model independent fit to the data. Since the differences of the logarithmic derivatives D_ℓ are determined by fitting the $\Delta(\theta_i)$ data, the proper relationship of $\sigma^+(\theta)$ to $\sigma^-(\theta)$ is enforced in the final adjustment of the average logarithmic derivatives S_ℓ to fit the combined $\sigma^+(\theta_i)$ and $\sigma^-(\theta_i)$ data. This constraint is absent from a conventional phase shift analysis that separately fits the cross sections for each pion charge. Otherwise the two methods are equivalent. The fact that the resulting fit parameters show a smooth and physically reasonable energy dependence, even though each energy was analysed separately, is viewed as further evidence in favor of these solutions.

The indicated errors in the tables are the deviations in each variable that produce a 10% increase in χ^2 with all the other variables held fixed. These are to be taken as a somewhat arbitrary, but scale independent, measure of the relative sensitivity of the fit to the various parameters. The conventional error estimates for fitted

parameters are the deviations that give unit increase in χ^2 above its minimum value, which is supposed to be less than the number of data points. This was thought inappropriate in the present case because of the mixed way the data was fit, and because of the large χ^2's obtained. Since we are doing a model independent fit equivalent to a phase shift analysis, the larger than expected χ^2 suggests underestimated data errors, possibly systematic. For example, the data points at $\theta = 80°$ consistently lie above the best fit cross sections for both charges, and the 100° points consistently lie below. These two angles account for nearly half the total χ^2 of the $\sigma_{\pm}(\theta)$ fits. When the 142.3 MeV/c $\sigma_{\pm}$ data was refitted without them, the χ^2 improved dramatically from 112 to 48, but the fitted values of S_ℓ hardly change (about 1%). It should be noted that this kind of systematic error, that affects both charges in the same way, tends to cancel out of the $\Delta(\theta)$ data that is used to determine the pion radius. In any case, the full data set was used in the final analysis.

IV. NUCLEAR INTERACTION MODELS

To interpret the empirical values of D_ℓ in Table 1 according to Eq. (35), we need a specific form, such as the optical model potential, for the nuclear interaction operator U_N, so that Eq. (21) can be integrated to provide a suitable internal wave function. In a multiple scattering theory derivation of the optical model,[15,17] the scattering wave function of a pion on a nucleus is constructed from the pion-single nucleon scattering amplitude and properties of the nuclear states, particularly the spacial density of nucleons. The optical potential is then defined as the equivalent interaction operator, acting on pion coordinates only, that generates the same elastic scattering amplitude.

In Watson's formulation,[15] the momentum space matrix elements of the optical potential are, in the impulse approximation, and with neglect of nuclear correlations,

$$\langle \underset{\sim}{k}' | U_N | \underset{\sim}{k} \rangle = \frac{1}{(2\pi)^3} \int d^3x \ \rho(x) \ e^{i(\underset{\sim}{k} - \underset{\sim}{k}') \cdot x} \cdot \left(-4\pi \ f(\underset{\sim}{k}, \underset{\sim}{k}') \right). \tag{42}$$

All that remains of nuclear structure in this formula is the density of nucleons $\rho(x)$, normalized so that $\rho(x)d^3x$ is the number of nucleons in the volume element d^3x. The amplitude, averaged over spin and isospin, for any one of them to scatter the pion from incident momentum $\underset{\sim}{k}$ to final momentum $\underset{\sim}{k}'$ is $f(\underset{\sim}{k}, \underset{\sim}{k}')$. The exponential provides that each volume element contributes with the proper phase to the total amplitude.

The coordinate space matrix elements of this optical potential are obtained by Fourier transformation. In Dirac notation $\left(\langle \underset{\sim}{r}|\underset{\sim}{k}\rangle = (2\pi)^{-3/2}\, e^{i\underset{\sim}{k}\cdot\underset{\sim}{r}}\right)$ we have

$$\langle \underset{\sim}{r}'|U_N|\underset{\sim}{r}\rangle = -4\pi \int d^3x\, \rho(\underset{\sim}{x}) \int d^3k \int d^3k'\, f(\underset{\sim}{k}, \underset{\sim}{k}')$$

$$\langle \underset{\sim}{r}'|\underset{\sim}{k}'\rangle\langle \underset{\sim}{k}'|\underset{\sim}{x}\rangle\langle \underset{\sim}{x}|\underset{\sim}{k}\rangle\langle \underset{\sim}{k}|\underset{\sim}{r}\rangle \quad . \tag{43}$$

Since $\langle \underset{\sim}{k}|\underset{\sim}{r}\rangle = \langle \underset{\sim}{r}|\underset{\sim}{k}\rangle^* = \langle \underset{\sim}{r}|-\underset{\sim}{k}\rangle$, and $\underset{\sim}{k}$ and $\underset{\sim}{k}'$ are dummy integration variables, we see by inspection that $\langle \underset{\sim}{r}'|U_N|\underset{\sim}{r}\rangle$ satisfies the symmetry condition of Eq. (28) provided

$$f(-\underset{\sim}{k}', -\underset{\sim}{k}) = f(\underset{\sim}{k}, \underset{\sim}{k}') \quad . \tag{44}$$

In terms of a partial wave expansion

$$f(\underset{\sim}{k}, \underset{\sim}{k}') = \sum_{\ell=0}^{\infty} (2\ell+1) a_\ell(k, k')\, P_\ell(\hat{k}' \cdot \hat{k}) \text{ with } k \equiv |\underset{\sim}{k}| \,,\ \hat{k} \equiv \underset{\sim}{k}/k \,, \tag{45}$$

this only requires the partial wave amplitudes be symmetric in k and k' :

$$a_\ell(k, k') = a_\ell(k', k) \quad . \tag{46}$$

This is trivially satisfied on the energy shell where $k = k'$. Thus the symmetry condition of Eq. (28), which is essential to the derivation of the key Eqs. (34) and (35), is translated in the optical model formalism

into a symmetry condition Eq. (46) on the off shell behavior of the pion nucleon partial wave amplitudes. In Eq. (44), this condition takes the form of an off shell extrapolation of time reversal invariance.

Kisslinger's optical potential is a convenient and widely used approximation to Eqs. (42) through (45). It consists of keeping only the first two partial waves of Eq. (45) in the form

$$-4\pi f(\underset{\sim}{k}, \underset{\sim}{k}') \cong b + c\, \underset{\sim}{k} \cdot \underset{\sim}{k} \quad , \tag{47}$$

where b and c are certain linear combinations of the S and P wave scattering lengths. All of the integrations in Eq. (43) may then be done explicitly, yielding finally an interaction operator whose effect in coordinate space representation is

$$\langle \underset{\sim}{r} | U_N | \psi \rangle = b\rho(\underset{\sim}{r})\, \psi(\underset{\sim}{r}) - c \underset{\sim}{\nabla} \cdot (\rho(\underset{\sim}{r})\, \underset{\sim}{\nabla} \psi(\underset{\sim}{r}) \quad . \tag{48}$$

The wave Eq. (21) then becomes

$$\left[\underset{\sim}{\nabla} \cdot (1 + \alpha(r))\, \underset{\sim}{\nabla} + k^2 - U(r) \right] \psi^t(\underset{\sim}{r}) = 2\eta k t\, v(r)\, \psi^t(\underset{\sim}{r}) \quad , \tag{49}$$

where $U(r) \equiv b\, \rho(r)$ is a local nuclear potential, and $\alpha(r) \equiv c\rho(r)$ is a non-local interaction term. The local nuclear interaction $U(r)$ is dominant in the S wave and is repulsive. The non-local interaction operator $-\nabla \cdot \alpha \nabla$ is attractive and dominates all higher partial waves. The Ericsons have refined the model, taking into account more details of nuclear structure and pion-nucleon interactions, but finding the same general form of wave equation.[17] For our purposes, b and c may be

considered complex phenomenological constants to be determined by the data. When Eq. (49) is resolved in partial waves by the substitution $\psi^t(\underline{r}) = \chi_\ell^t(r)\, Y_\ell^m(\Omega)$ the resulting radial equation is

$$\frac{d}{dr}\left[r^2(1+\alpha)\ \frac{d\chi_\ell^t}{dr}\right] + r^2\left[k^2 - U(r) - 2\eta k t v(r) - (1+\alpha(r))\ \frac{\ell(\ell+1)}{r^2}\right]\chi_\ell^t(r) = 0 \quad . \qquad (50)$$

It is evident from the form of Eq. (50) that both χ_ℓ and the quantity $\phi_\ell \equiv r^2(1+\alpha)\ \frac{d\chi_\ell}{dr}$ must be continuous everywhere, and so (except where $\chi_\ell = 0$) must be

$$\lambda_\ell^t(r) \equiv 1 + \phi_\ell^t(r)/\left(r\chi_\ell^t(r)\right) = 1 + (1+\alpha)\ \frac{r\chi'}{\chi} \quad . \qquad (51)$$

This generalized logarithmic derivative is consistent with Eq. (23) at the boundary $r = R$ where $\alpha(R) = 0$.

We take a Gaussian form

$$\rho(r) = A\,\pi^{-3/2}\,a_N^{-3}\ \exp\left(-r^2/a_N^2\right) \quad , \qquad (52)$$

for the Helium nucleon density, and assume it has the same extent ($a_N = 1.34$ F) as the observed charge distribution. (Fig. 1). With $b = b_1 + ib_2$ and $c = c_1 + ic_2$, there are 4 real parameters to be determined. Computer programs were written to numerically integrate Eq. (50) for $t = 0$ with the expectation that b and c could be adjusted

so that the calculated λ_ℓ^0 would match the complex empirical values of S_ℓ for the S and P waves listed in Table I. (Some of the formulas used are discussed in appendix B.) As expected, b was determined mainly by S_0, and c_1 by Re S_1. For these values of b and c_1 however, there was no value of c_2 that would give the empirical value of Im S_1, essentially because of a discontinuity in λ_ℓ at $c_2 = 0$. There is, in effect, an intrinsic imaginary part to λ_ℓ, having the same sign as c_2, that remains even in the limit $b_2 = 0$, $c_2 \to 0$. Consequently, as c_2 passes through zero in the search routine, Im λ_1 jumps from a value well below Im S_1 to a value well above it; the empirical value lies in the excluded region. The source of this discontinuity is shown in the appendix to be the singular point r_o in the radial Eq. (50) where $1 + \alpha(r_o) = 0$. If $c_2 = 0$, and $\alpha(0) = c_1\rho(0) < -1$, r_o will be in the nuclear surface where the density has fallen to the value $\rho(r_o) = -1/c_1$. (From Table III, we have Re $\alpha(0) \simeq -2$) The radial wave function in this case has a logarithmic branch point at r_o, and so an imaginary part for $r > r_o$ whose sign depends on how the singularity is handled. In general the singular point will be at the complex value of r_o for which $\rho(r_o) = -1/(c_1 + ic_2)$, but for small c_2 will still lie very near the path of integration along the real r axis from 0 to R, and will still have a profound effect on the wave function. In particular, the intrinsic imaginary part to the logarithmic derivatives calculated from the Kisslinger model means that b_2 and c_2 are really arbitrary, and cannot be determined by fitting absorbtion data.

Even though the Im S_1 listed in Table I are not really well determined by the data, this is still a serious difficulty in principle

with the Kisslinger model, at least as it applies to Helium. It means that, when this wave function branch point effect occurs, the Kisslinger model cannot properly account for absorbtion phenomena.

For our present purposes however, all we really require is a set of radial wave functions $\chi_\ell^0(r)$ $(l = 0,1,2)$ satisfying the boundary conditions $\lambda_\ell^0 = S_\ell$, to be used to interpret the empirical D_ℓ's according to Eq. (35). To this end, we have adopted the following ad hoc procedure. The imaginary part of the P wave logarithmic derivative, Im S_1, was temporarily replaced by a fake value Im S_1' large enough to permit a solution for (b,c) that satisfies the corresponding modified S and P wave boundary conditions. The result is given in the first 3 columns of Table III. Then with c fixed at the value so determined, the complex parameter b was readjusted separately for each partial wave to exactly satisfy the original empirical boundary conditions. For the S wave there was, of course, no change in b. For the P and D waves we find $b_2 > 0$, to partially cancel the anomalously large negative Im S_ℓ resulting from the singular point. These values are given in the last two columns of Table III. We refer to this solution in the next section as the "modified Kisslinger model". At 142.3 MeV/c, a fit was also done with $a_N = 1.27$ F as a check on the sensitivity to nuclear density.

For a simple alternative solution, the same programs were used with $c \equiv 0$ to fit a local potential to each partial wave. The parameters of this local model are given in Table IV. Fig. 5 shows the real part of fitted weighting functions

$$\left(y_\ell^0(r)\right)^2 \equiv \left[r\,\chi_\ell^0(r) \,/\, R\,\chi_\ell^0(R)\right]^2$$

for both models at 142.3 MeV/c. The peculiar bump in the Kisslinger model wave functions, occuring at $r = r_o = 1.1F$ for $a_N = 1.34F$, is another manifestation of the singular point Re $\alpha = -1$. The local potential solutions are well behaved as expected. Since the true physical wave function presumably does not have logarithmic branch points, even if the local potential interaction itself is unrealistic, the weighting functions it generates may be the most realistic, especially since all possible weighting functions must satisfy the empirical boundary conditions of Eq. (36). In fact, Lepore and Riddell have shown by direct numerical solution in momentum space of the partial wave Schrödinger equation for the optical model interaction Eq. (42) that the singular point effects in the wave function disappear if the coefficients (b, c) of Eq. (47) are given a gradual cutoff for large k and k'.[18]

V. DETERMINATION OF THE PION RADIUS

Given an internal wave function $y_\ell^0(r)$ that satisfies the conditions of Eq. (36), and a formula such as Eq. (18) or (20) for the internal Coulomb potential $v(r)$, we may calculate D_ℓ as a function of r_π. Since we have two nuclear models (Kisslinger and local) and two pion shapes (Gaussian and Yukawa), there are four cases to consider. Fig. 6 shows the calculated ReD_ℓ vs r_π at 142.3 MeV/c for the first 3 partial waves. The calculated curves for free waves (i.e. $\chi_\ell(r)$ = spherical bessel function) are also included to show the effect of wave function distortion by the nuclear force. The nuclear force is repulsive in the S wave, attractive in higher waves. This results in a decrease in ReD_0 and an increase in ReD_ℓ for $\ell \geq 1$ from their free wave values. To show the dependence on the pion model, the S wave curves are drawn for both pion charge distributions. The two distributions are of course identical at $r_\pi = 0$, but for large pion radius, the Yukawa model(Eq. (20)) gives the larger value of D_ℓ, corresponding to a deeper central value of the Coulomb potential. The effect of the nuclear model on the calculated values of D_ℓ is also exhibited. For the same internal Coulomb potential, the modified Kisslinger model wave function yields a value of ReD_0 some 6% larger than the local model. For the P and D waves, where the internal wave function is more dominated by the centrifugal potential, the nuclear model dependence of ReD_ℓ is 2.8% and 1.6% respectively.

The horizontal bands are the empirical values of ReD_ℓ from Table I, with the deviations that cause a 10% increase in χ_Δ^2. The

pion radius for each model may be read from the intersection of the computed curve for ReD_0 with the data band. This indicates a surprisingly large pion radius of between 2 and 3 F . With the pion radius so determined, the calculated ReD_ℓ for the P and D waves lies somewhat above the corresponding data bands. Nevertheless, the numerical agreement is close enough to be taken as some confirmation of the basic Eqs. (34, 35, and 36). Note that without the wave function distortion by the nuclear force, there would be no agreement on the value of r_π among the partial waves.

For a data fit completely consistent with a given model, we compute D_ℓ for all partial waves as a function of pion radius, and using the empirical values of S_ℓ from Table I, plot χ_Δ^2 vs. r_π (Fig. 7). The values of χ_Δ^2 and r_π at the minima, with the deviations Δr_π that cause a 10% increase in χ_Δ^2 for the various models, are listed in Table V. Some of these values of r_π are also shown in Fig. 6. The minimum values of χ_Δ^2 are larger than for the model independent fit of Table I because of the additional constraint: the P wave is well determined by the precise data in the minimum, and it disagrees slightly with the calculated value for each model. The following remarks may be made about Fig. 6 and Table V :

(i) The 142.3 MeV/c data again has the highest χ_Δ^2 (around 60 for 15 data points), but has the sharpest minima, reflected in the size of the Δr_π.

(ii) The modified Kisslinger model gives pion radii about .4 - .6 F larger than the local model with the same pion form. Since the wavefunctions generated by these two models are about as different

as possible within the constraints imposed by the boundary conditions at $r = 0$ and $r = R$, we may estimate that the uncertainty in r_π due to the nuclear model dependence is $\lesssim 0.6$ F.

(iii) In the 2 to 3 F range, with a given nuclear model, the exponential pion model indicates an r_π about 0.2 - 0.5 F bigger than the Gaussian pion model. This is a measure of the uncertanity in r_π due to choice of pion shape.

(iv) All four energies are consistent, with perhaps a slight tendency for the higher energies to require a bigger r_π to fit.

Figure 4 shows that data and calculated values of $\Delta(\theta)$ at each energy for the best model independent fits (Table I). The curves for the best model dependent fits (Tables III, IV, V) are very similar, although they give somewhat higher χ^2s. The curves for $r_\pi = 0$ calculated with the fitted Kisslinger model wave functions are shown for comparison. These gave the highest calculated χ^2s (cf. Fig. 7). All this shows that $\Delta(\theta)$ is too small in the forward direction, or correspondingly, that $\sigma_+(\theta)$ is too close to $\sigma_-(\theta)$ to permit a small value of r_π.

VI. CONCLUSION

Within our basic assumption that the Coulomb potential Eq. (15) is the only charge dependent interaction in the generalized Klein Gordon Eq. (21), data analysis indicates a surprisingly large r_π of 2 to 3 F. The boundary condition method effectively reduces the uncertainty in r_π due to nuclear model dependence to about the level of the uncertainty due to experimental statistics. The use of the exact external $(r > R)$ solution of the radial wave equation avoids the long range Coulomb divergence difficulties. Evidently then, the large pion radius result is inherent in the data and our basic theoretical assumption (Eqs. 15, 21), and is not due to either calculational difficulties or the detailed choice of nuclear interaction model. In view of the disagreement with the simple vector dominance model prediction of $r_\pi = 0.63$ F, some comments on possible alternatives are in order:

(i) We have taken relativity explictly into account only in the kinematics used to calculate k and η. Only the instantaneous (Coulomb gauge) electrostatic potential is included in the equation of motion. The magnetic field seen in the center of mass (CM) system due to the recoil motion of the nucleus is neglected. Rix and Thaler[19] suggest that k and η be chosen for the relativistic two body problem so that the pure Coulomb amplitude Eq. (7) agrees to first order with the covariant Feynman Born amplitude for the electromagnetic interaction of two spinless bosons. This leads to $2k\eta = 2Ze^2(E_1E_2 + k^2)/(E_1 + E_2)$, where E_1, E_2 are the CM energies of the two particles, and k is the CM momentum. Our formula differs only in the absence of the k^2 term from the numerator. (This k^2 term presumably represents the

magnetic contribution.) Another alternative would be to neglect nuclear recoil motion, and use the Lab momentum and velocity of the pion to compute (k, η). Magnetic interaction would then be strictly zero, and the Klein Gordon equation in a Coulomb field would govern the long range motion of the pion. Both these alternatives give a value of η about 2 to 3% larger than ours, and lead ultimately to a small increase in the measured value of r_π.

(ii) The assumption of exact charge independence of the nuclear interaction operator is crucial to this whole approach to the measurement of r_π. If the nuclear interaction of π^+ differed slightly from that of π^-, there would be a direct strong interaction contribution to the logarithmic derivative difference D_ℓ (Eq. 25). Let $U_N^{\pm}$ be the nuclear interaction operator for $\pi^{\pm}$, and assume that the difference $\Delta U_N \equiv U_N^{+} - U_N^{-}$ is a local operator. Then, by the derivation leading to Eq. (35), we have $D_\ell \rightarrow D_\ell^{c}(r_\pi) + D_\ell^{S}$, where $D_\ell^{c}(r_\pi)$ is the pion radius dependent Coulomb contribution given by Eq. (35), and D_ℓ^{S} is an additional strong charge asymmetry contribution given by

$$D_\ell^{S} = \frac{R}{2\eta} \int_0^R \Delta U_N(r) \left[y_\ell^{0}(r) \right]^2 dr \quad . \qquad (53)$$

The experimental values of D_ℓ from Table I are now to be interpreted according to

$$D_\ell^{\text{Expt.}} = D_\ell^{c}(r_\pi) + D_\ell^{S} \quad . \qquad (54)$$

Any combination of r_π and ΔU_N that satisfies Eq. (54)[via Eqs. (35) and 53)] will agree with the data. The values of r_π given in Table V are based on the assumption that $D_\ell^S = 0$. Since D_ℓ^c is a decreasing function of r_π (Fig. 6), we require in general $D^S \leq 0$ ($U_N^+ \leq U_N^-$) to fit the data with smaller values of r_π. For example, using the local model wave functions, it would require $\mathrm{Re}D_0^S \cong -1.13$ to bring the 142.3 MeV/c S wave data into agreement with $r_\pi = 0.63$ F. Evaluation of Eq. (53) on the assumption that $U_N^\pm(r) = (b \pm \frac{1}{2}\Delta b)\rho(a_N;r)$, where $b = 1.1$ F from Table IV, and $\rho(a_N;r)$ is given by Eq. (52), then leads to a fractional strength difference $\Delta b/b = +.073$ $D_0^S = -.083$. Similiarly, if $U_N^\pm(r) = b\rho(a_N \pm \frac{1}{2}\Delta a\,;\,r)$,[20] we have to lowest order a fractional range difference $\Delta a/a_N \cong -.10$ $D_0^S = +.113$. At least for these simple models then, roughly a 10% violation of strong interaction charge independence is required to bring our fit into agreement with the vector dominance model prediction for r_π.

(iii) Finally, although the simple ρ pole term of the vector dominance model Eq. (19a) may well represent the pion form factor for the large timelike four momentum transfers near the pole, it is not necessarily sufficient for the small spacelike q^2 considered here. See, e.g. Ref. 19 for an estimate that inclusion of the contribution of the $A_1(1^+)$ meson leads to $r \sim 1.4$ F.

ACKNOWLEDGMENTS

I would like to express my appreciation to Dr. R. J. Riddell, Jr. for the initial suggestion and extensive advice, support, and encouragement in the course of this work; to Dr. K. M. Crowe, Mr. A. Fainberg, and Dr. A. S. L. Parsons for many very useful discussions and the use of their data in advance of publication; and to Dr. J. V. Lepore for numerous helpful conversations.

APPENDIX

A. Simple Relativistic Reduced Mass Formalism

The Klein Gordon equation describing the motion of a particle of mass m and total energy E in a fixed electrostatic potential $V(r)$ may be written

$$-\nabla^2\psi(r) = \left[k^2 - 2EV(r) + V^2(r)\right]\psi(r) \quad , \qquad (A1)$$

where $k^2 = E^2 - m^2$. This is used, for example, to calculate wave-functions of a pion in the Coulomb field of a heavy nucleus. The assumption of fixed potential then corresponds to neglect of nuclear recoil motion. To include this recoil motion requires in principle the solution of a two body problem. This is easily accomplished in the non-relativistic limit where the introduction of center of mass and relative coordinates reduces it to a pair of one body problems. In the center of mass (CM) system, the relative coordinate $\underset{\sim}{r} = \underset{\sim}{r}_1 - \underset{\sim}{r}_2$ of the two particles (masses m_1, m_2) varies as if it were the coordinate of a single particle having the reduced mass

$$\mu_{NR} = m_1 m_2/(m_1 + m_2) \quad , \qquad (A2)$$

and moving with the actual available energy E_{CM} in the fixed interaction potential $V(r)$. The fully covariant two body problem however is in principle much more difficult, and is not attempted here. Nevertheless, for many applications a simple generalization to relativistic kinematics of the familiar reduced mass formalism outlined above would be useful. One such generalization is suggested in the following.

We begin by reviewing the nonrelativistic case in a form that has an easy relativistic analog. In the center of mass system where both particles have momentum of magnitude p, the total kinetic energy is

$$T_{CM} = \frac{p^2}{2m_1} + \frac{p^2}{2m_2} = E_{CM} - V(r) \quad . \qquad (A3)$$

The reduced mass μ_{NR} is, by definition, the mass a single particle must have if its momentum is p and its kinetic energy T_{CM}, i.e. $\mu_{NR} \equiv p^2/2T_{CM}$. Its role in the equation of motion is to give a single particle like appearence to the actual relation of p to E_{CM} and $V(r)$:

$$p^2 = 2\mu_{NR}\left(E_{CM} - V(r)\right) \quad . \qquad (A4)$$

On quantization in the coordinate basis, p^2 is represented by $-\nabla^2$, and Eq. (A4) becomes the time independent Schrödinger equation for a particle of mass μ_{NR} and energy E_{CM} in a fixed potential $V(r)$.

$$-\nabla^2\psi(r) = 2\mu_{NR}\left(E_{CM} - V(r)\right)\psi(r) \quad . \qquad (A5)$$

The wave function $\psi(r)$ satisfying Eq. (A5) is interpreted as the probability amplitude for the interparticle seperation r. Now for a relativistic analog of Eq. (A3) we assume that in the CM system, the momentum p of either particle satisfies

$$W = \left(p^2 + m_1^2\right)^{1/2} + \left(p^2 + m_2^2\right)^{1/2} + V(r) \quad , \qquad (A6)$$

where W is the total energy, including rest energy $m_1 + m_2$.

Equation (A6) may be solved for the classical momentum p as a function of r, yielding

$$p^2 = F(r) \quad , \tag{A7a}$$

$$F(r) \equiv \frac{\left[(W - V(r))^2 - (m_1 + m_2)^2\right]\left[(W - V(r))^2 - (m_1 - m_2)^2\right]}{4(W - V(r))^2} \quad . \tag{A7b}$$

This is the relativistic analog of Eq. (4). The corresponding wave equation is

$$-\nabla^2\psi(\underset{\sim}{r}) = F(\underset{\sim}{r})\ \psi(\underset{\sim}{r}) \quad . \tag{A8}$$

In order to compare Eq. (A7) and (A8) with the relativistic single particle Eq. (A1), we expand $F(r)$ in powers of the potential $V(r)$:

$$F \equiv F_0 + F_1 V + F_2 V^2 + R(V) \tag{A9a}$$

where

$$F_0 = \frac{\left[W^2 - (m_1 + m_2)^2\right]\left[W^2 - (m_1 - m_2)^2\right]}{4W^2} \quad , \tag{A9b}$$

$$F_1 = -2\left[\frac{W^4 - (m_1^2 - m_2^2)^2}{4W^3}\right] \quad , \tag{A9c}$$

$$F_2 = \frac{W^4 + 3(m_1^2 - m_2^2)^2}{4W^4} \quad , \tag{A9d}$$

and

$$R(V) = \frac{(m_1^2 - m_2^2)^2 \ (4W - 3V)}{4W^4 \ (W - V)^2} \ V^3 \ . \qquad \text{(A9e)}$$

Equation (A9) is easily verified to be an exact algebraic identity. Comparison with Eq. (A1) indicates that the asymptotic[22] momentum of the equivalent single particle is given by $k^2 = F_0 = \lim_{V \to 0} F(r)$. This is the usual relativistic formula for the barycentric momentum of two free particles with total energy W. Of course it also follows directly from $W = E_1 + E_2$ where the asymptotic single particle energies E_i are given by

$$E_1 = \left(k^2 + m_1^2\right)^{\frac{1}{2}} = \frac{W^2 + m_1^2 - m_2^2}{2W} \ , \qquad \text{(A10a)}$$

$$E_2 = \left(k^2 + m_2^2\right)^{\frac{1}{2}} = \frac{W^2 + m_2^2 - m_1^2}{2W} \ . \qquad \text{(A10b)}$$

The terms linear in V define the equivalent particle energy as

$$E \equiv -\frac{1}{2} F_1 = \frac{W^4 - (m_1^2 - m_2^2)^2}{4W^3} \ . \qquad \text{(A11)}$$

With use of Eq. (A10) this may be rewritten as a "reduced energy"

$$E = \frac{E_1 E_2}{E_1 + E_2} \ . \qquad \text{(A12)}$$

The terms higher than 2nd order in V are collected in the explicit remainder

$$R(V) = \left\{ \left(1 - \frac{4E}{W}\right) \frac{\left(1 - \frac{3}{4} \cdot \frac{V}{W}\right) \cdot \frac{V}{W}}{\left(1 - \frac{V}{W}\right)^2} \right\} V^2 \quad . \tag{A13}$$

For potentials $V \ll W$ (the usual case), this remainder may be treated as a small perturbation, or neglected entirely. Then Eq. (A8) may be approximated by

$$-\nabla^2 \psi(\underset{\sim}{r}) = \left[k^2 - 2E\, V(\underset{\sim}{r}) + \left(1 - \frac{3E}{W}\right) V^2(\underset{\sim}{r})\right] \psi(\underset{\sim}{r}) \quad , \tag{A14}$$

where the definition of E has been used to simplify the V^2 term. Equation (A14) is the relativistic analog of Eq. (A5): both represent the reduction of relative motion in a two body system to an equivalent one body system. The reduction is exact in the nonrelativistic case, but only approximate in the relativistic case. In particular, the V^2 term in Eq. (A14) is somewhat smaller than in Eq. (A1), and terms of order $\frac{V^3}{W}$ have been omitted.

In the nonrelativistic case, the introduction of center of mass and relative coordinates may be done with equal result either before or after quantization. The same may not be said for the relativistic case. See Goldberger and Watson[23] for a discussion of the conditions on V under which the Schrödinger equation for the scattering of a relativistic beam particle on a massive (nonrelativistic) target may be reduced

to an equivalent one body equation similar to Eq. (A14).

The definition Eq. (A12) of the equivalent energy also has the reasonable consequence that the asymptotic velocity $\beta = k/E$ of the equivalent particle is just the asymptotic relative velocity of the two actual particles:

$$\beta = \beta_1 + \beta_2 \quad \text{where} \quad \beta_i = k/E_i \quad . \tag{A15}$$

If a single free particle were to have momentum k and total energy E, its mass would have to be

$$\mu(k^2) = \left(E^2 - k^2\right)^{1/2} = E\left(1 - \beta^2\right)^{1/2} . \tag{A16}$$

With the E and k given above, Eq. (A16) defines a relativistic analog of the reduced mass. It has in general a rather complicated momentum dependence, but obviously approaches μ_{NR} (Eq. (A2)) for $k \ll m_1, m_2$. Note however that only E and k appear in the wave Eq. (A14); μ itself is not needed.

Equation (A14) is based entirely on the assumption that Eq. (A6) holds in the barycentric system. No comment on the Lorentz transformation properties of V is intended beyond the remark that the other terms in Eq. (A6) are the time components of four- vectors, as is the V in Eq. (A1). Although its derivation is rather heuristic, Eq. (A14) has the following desirable properties:

(a) It is symmetric in the masses m_1, m_2.

(b) For $m_1, m_2 \gg k, V$, it becomes the Schrödinger Eq. (A5) with reduced mass μ_{NR}.

(c) For $m_2 \gg m_1$, k,V, it becomes the Klein Gordon Eq. (A1) for a particle of mass m_1 in a fixed potential V(r).

(d) As $V \to 0$, it reproduces the standard barycentric relativistic kinematics of two free particles of any energy.

We therefore adopt Eq. (A14) as a generalization of the Klein Gordon equation to include the kinematic effects of the recoil motion of the target nucleus. For our problem (~150 MeV/c pions on He^4) neglect of this nuclear recoil motion leads to about a 5% increase in k, and a 2.5% increase in the Coulomb parameter $\eta = \mathbf{Z}\alpha/\beta$. We have $m_1 = m_\pi = 139.6$ MeV, $m_2 = M_{He} = 3727.6$ MeV and $V_C(r) \lesssim 2$ MeV. Therefore the remainder term $R \lesssim 4 \times 10^{-4} V^2$ and $V^2 \lesssim 2 \times 10^{-4} k^2$, so both are neglected in Eq. (1) of the text.

APPENDIX

B. Some Computational Techniques for the Kisslinger Model

In this appendix, we list some formulas useful in the practical problem of integrating the Kisslinger model radial equation and adjusting the nuclear interaction parameters to make the resulting wave function satisfy assigned boundary conditions at some radius R just outside the nucleus. Local potential models are of course included as the special case where the gradient interaction function $\alpha(r)$ is identically zero. It is convenient for the following derivations to split the Kisslinger model radial equation Eq. (50) of the text into a pair of coupled linear first order differential equations:

$$\psi(r) = r^2\left(1 + \alpha(r)\right) \frac{dX}{dr} \quad , \tag{B1a}$$

and

$$\frac{d\psi}{dr} = Q(r)X(r) \quad , \tag{B1b}$$

where

$$Q(r) \equiv r^2\left(U(r) - k^2\right) + \ell(\ell + 1)\left(1 + \alpha(r)\right) \quad . \tag{B1c}$$

This form was also necessary for the numerical integration routine (Berkeley ZAM) that was available. Given ℓ, k^2, $U(r)$, and $\alpha(r)$, this routine was set up to generate the solution with the form $X(r) \sim \text{const.} \times r^{\ell}$ near the origin $(r = 0)$. The logarithmic derivative of this wave function, defined as (cf. Eq. (51) of text)

$$\lambda \equiv 1 + (1 + \alpha) \left. \frac{r\chi'}{\chi} \right|_{r=R} = 1 + \psi(R)/(R\chi(R)) \ , \qquad (B2)$$

depends implicitly on the choice of $U(r)$ and $\alpha(r)$. To investigate the changes in λ due to changes in (U,α), we compare the solution (χ,ψ) of Eq. (B1) with the solution $(\hat{\chi},\hat{\psi})$ generated by an alternate choice $(\hat{U},\hat{\alpha})$:

$$\hat{\psi} = r^2(1 + \hat{\alpha})\,\hat{\chi}' \ ; \quad \hat{\psi}' = \hat{Q}\,\hat{\chi} \ ; \quad \text{etc.} \ . \qquad (B3)$$

By usual multiplication of Eq. (B1b) by $\hat{\chi}$, Eq. (B3b) by χ, and subtraction we have

$$\hat{\chi}\,\psi' - \chi\hat{\psi}' = (Q - \hat{Q})\,\hat{\chi}\chi \ . \qquad (B4a)$$

Use of Eqs. (B1a) and (B3a) allows this to be rewritten as

$$\frac{d}{dr}\,(\hat{\chi}\psi - \chi\hat{\psi}) = (Q - \hat{Q})\hat{\chi}\chi + r^2(\alpha - \hat{\alpha})\,\hat{\chi}'\,\chi' \ . \qquad (B4b)$$

Integration from 0 to R, and division by $R\hat{\chi}(R)\,\chi(R)$ then results in an exact formula for the logarithmic derivative shift due to the change $(U,\alpha) \to (\hat{U},\hat{\alpha})$:

$$\lambda - \hat{\lambda} = \left(I_U(R) + I_\alpha(R)\right) / \left(R\hat{\chi}(R)\,\chi(R)\right) \ , \qquad (B5a)$$

where

$$I_U(R) \equiv \int_0^R \left[U(r) - \hat{U}(r)\right] r^2\,\hat{\chi}(r)\,\chi(r)\,dr \ , \qquad (B5b)$$

and

$$I_\alpha(R) \equiv \int_0^R \left[\alpha(r) - \hat{\alpha}(r)\right]\left[\ell(\ell+1)\hat{\chi}(r)\chi(r) + r^2 \hat{\chi}'(r)\,\chi'(r)\right] dr \quad . \tag{B5c}$$

This general formula has several interesting special cases:

(i) If $\hat{\alpha}(r) = \alpha(r)$, $\hat{U}(r) = U_N(r) + t'2\eta kv(r)$ and $U(r) = U_N(r) + t\,2\eta kv(r)$, then Eq. (B5) reduce to Eq. (30) of the text, leading directly for this model to the formula (Eq. 35) for the Coulomb difference D_ℓ.

(ii) With the same (U,α), but $\hat{\alpha} = \hat{U} = 0$, the comparison solution is just the spherical bessel function: $\hat{\chi}(r) = j_\ell(kr)$. Then, after a partial integration on I_α (utilizing Eq. (B3b) and assuming $\alpha(R) = 0$), Eq. (B5) yield an integral representation for the neutral ($t = 0$) logarithmic derivative in terms of the normalized internal wave function $y(r) = r\chi(r) \,/\, R\chi(R)$:

$$\lambda = 1 + \frac{kRj'_\ell(kR)}{j_\ell(kR)} + \int_0^R dr\, y(r) \left[\frac{rj_\ell(kr)\left(U_N(r) + k^2\alpha(r)\right) - krj'_\ell(kr)\alpha'(r)}{j_\ell(kR)}\right]. \tag{B6}$$

Of course if $\chi(r)$ were known, λ would be given by Eq. (B2). But conversly if λ were the known quantity (e.g. Table I), $y(r)$ would be strongly constrained (cf. Eq. (36) of text) and Eq. (B6) could be used to display the contribution to λ of the various terms in the wave equation. Similar formulas for the other charges ($t = \pm 1$) may be

derived using $\hat{U}(r) = 2\eta kt/r$. Then $(kr)j_\ell(kr)$ is replaced by the regular Coulomb function $F_\ell(t\eta;kr)$, and Eq. (B6) has an additional Coulomb term.

(iii) Suppose U and α depend on a set of parameters $s = (s_1, s_2, \ldots, s_n)$: $U = U(s;r)$ and $\alpha = \alpha(s;r)$. Then the logarithmic derivative $\lambda(s)$ will also depend on these parameters, and Eq. (B5) may be used to construct the derivatives $\partial\lambda/\partial S_i$ from a single calculation of the wave function $\chi(s;r)$. This permits the use of efficient gradient type iteration methods to adjust the parameters to match an assigned value of λ. Taking $\hat{U} = U(\hat{s};r)$ and $\hat{\alpha} = \alpha(\hat{s};r)$ where $\hat{s} = (s_1, s_2, \ldots, s_i + \Delta s_i, \ldots, s_n)$, in the limit $\Delta s_i \to 0$ we have

$$\hat{\chi} = \chi(\hat{s};r) \longrightarrow \chi(s;r)$$

and

$$\frac{\partial\lambda}{\partial s_i} = \frac{1}{R\chi(R)^2} \int_0^R dr \left\{ \left[r\chi(r)\right]^2 \frac{\partial U}{\partial s_i} + \left[\ell(\ell+1)\chi(r)^2 + \left(r\chi'(r)\right)^2\right] \frac{\partial\alpha}{\partial s_i} \right\} . \qquad \text{(B7)}$$

In Sec. IV we used $U(r) = (b_1 + ib_2)\,\rho(r)$ and $\alpha(r) = (c_1 + ic_2)\rho(r)$. The parameter set is $s = (b_1, b_2, c_1, c_2)$, and Eq. (B7) was used with $\partial U/\partial b_1 = \rho(r)$, etc., to fit the calculated λ's to the empirical ones. Note that if U and α are analytic functions of a complex variable

$z = s_1 + is_2$, and so satisfy the Cauchy-Riemann conditions ($\partial U/\partial s_2 = i\partial U/\partial s_1$, etc.), then $\lambda(z)$ is also analytic in z because it also satisfies these conditions. The one restriction to be observed is that if the parameters are such that $X(s;r)$ has a branch cut (cf. Appendix C), $\hat{s}$ and s must be chosen on the same side of the cut to achieve $\hat{X} \to X$ in the limit $\hat{s} \to s$. In this connection, note that substituting the complex conjugates of U and α into Eq. (B1) does not necessarily generate the complex conjugate of X. Therefore use of Eq. (B5) to construct $\lambda - \lambda^* = 2i\ \mathrm{Im}\ \lambda$ must be done with caution. These restrictions are not necessary if $\alpha(r) > -1$ everywhere, as in the special case of local potential models where $\alpha(r) \equiv 0$.

APPENDIX

C. Analysis of the Kisslinger Model Singular Point for Real $\alpha(r)$.

The radial Schrödinger Equation for the Kisslinger model of pion-nucleus interactions has the general form

$$\frac{d}{dr}\left[r^2\left(1+\alpha(r)\right)\frac{dX}{dr}\right] + \left[r^2\left(k^2 - U(r)\right) - \left(1+\alpha(r)\right)\ell(\ell+1)\right]X = 0 \quad . \tag{C1}$$

The complex non-local interaction coefficient $\alpha(r)$ is in general proportional to the nuclear density $\rho(r)$, and vanishes outside the nucleus. We take for simplicity $\alpha(r) = c\rho(r)$ where $c = c_1 + ic_2$ is a complex constant. The essential features of the following argument remain valid, however, for more complicated forms of $\alpha(r)$ such as those given in Ref. 17. Equation (1) has a singular point r_o where $1 + \alpha(r_o) = 0$. If $c_2 = 0$, and $\alpha(0) = c_1\rho(0) < -1$, this singular point will be in the nuclear surface where the density has fallen to the value $\rho(r_o) = -1/c_1$. If $c_2 \neq 0$, the singular point will be at the complex value of r_o where $\rho(r_o) = -1/c = (-c_1 + ic_2)/|c|^2$. For the Gaussian density distribution, and presumably in general, Im r_o has the opposite sign from c_2: for $c_2 < 0$, r_o lies above the real r axis, and comes down onto the axis as $c_2 \to 0$.

To investigate the effect of this singular point on the Kisslinger radial wave function, we apply the classical analysis of second order linear differential equations as given in Ref. 24. Writing the radial equation in the form

$$X'' + p(r)\,X' + q(r)\,X = 0 \quad . \tag{C2}$$

we find that both

$$p(r) \equiv \frac{2}{r} + \frac{\alpha'(r)}{1 + \alpha(r)} \quad \text{and} \quad q(r) \equiv \frac{k^2 - U(r)}{1 + \alpha(r)} - \frac{\ell(\ell + 1)}{r^2} \quad , \tag{C3}$$

have first order poles at $r = r_o$. Substitution of power series expansions about r_o for $(r - r_o)\, p(r)$ and $(r - r_o)^2\, q(r)$, and the form

$$y(r) = (r - r_o)^{\beta} \left[1 + \sum_{m=1}^{\infty} a_m (r - r_o)^n \right] , \tag{C4}$$

for X into Eq. (C2) then yields a set of recursion formulas for the a_n. The first of these is the indicial equation which turns out to be $\beta^2 = 0$. Therefore $y(r)$ is analytic at r_o:

$$y(r) = 1 + a_1(r - r_o) + a_2(r - r_o)^2 + \ldots , \tag{C5}$$

and, since the indicial equation has equal roots, the second independent solution must be sought by variation of parameters. Writing it in the form $w(r) = \xi(r) y(r)$, we find on substitution in Eq. (C2) that

$$\frac{d\xi}{dr} = \frac{1}{r^2 \left(1 + \alpha(r)\right) y^2(r)} \quad . \tag{C6}$$

This means that since $1 + \alpha(r)$ has a simple zero at r_o, $\xi'(r)$ has a simple pole there, and $\xi(r)$ has a logarithmic branch point. The general solution of Eq. (C2)

$$\chi(r) = \big(A + B\xi(r)\big)y(r) \quad , \tag{C7}$$

where A and B are arbitarary constants, then also has a logarithmic branch point at r_o (unless B =0). Now the physical solution of the radial equation must start at the origin as $\chi(r) \simeq \text{const.} \times r^{\ell}$. We want to propagate this solution outward along the real r axis to the boundary r = R, using the form (C7) to cross the singular point. The constants (A,B) are determined by the continuity of $\chi(r)$ and $\psi(r) \equiv r^2\big(1 + \alpha)\big)\chi'(r)$ at $r = r_1 \equiv r_o - \Delta r$:

$$B = y(r_1)\ \psi(r_1) - r_1^{\,2}\big(1 + \alpha(r_1)\big)y'(r_1)\ \chi(r_1) \quad ,$$

$$A = \chi(r_1)/y(r_1) - B\xi(r_1) \quad . \tag{C8}$$

Since $y(r)$ and $\chi(r)$ both satisfy Eq. (C2), B is actually independent of r_1. The same continuity conditions are used again at $r = r_2 \equiv r_o + \Delta r$ to obtain the values of $\chi(r_2)$, $\psi(r_2)$ needed to continue the integration:

$$\chi(r_2) = \frac{y(r_2)}{y(r_1)} \cdot \chi(r_1) + y(r_2)B\big(\xi(r_2) - \xi(r_1)\big) \quad ,$$

$$\psi(r_2) = \frac{1}{y(r_2)} \left[B + r_2^{\,2}\big(1 + \alpha(r_2)\big)y'(r_2)\ \chi(r_2)\right] \quad . \tag{C9}$$

We therefore must somehow evaluate the singular integral

$$I(\Delta r) \equiv \xi(r_2) - \xi(r_1) \equiv \int_{r_o - \Delta r}^{r_o + \Delta r} \frac{dr}{r^2\left(1 + \alpha(r)\right) y(r)^2} \quad . \tag{C10}$$

The pole at $r = r_o$ may be explicitly separated by a partial fraction expansion of the integrand. Writing the denominator in the form (with $z = r - r_o$)

$$r^2\left(1 + \alpha(r)\right) y(r)^2 \equiv z\left(g + z\, h(z)\right) \quad , \tag{C11}$$

we have $g = r_o^2 \alpha'(r_o)$, and $h(z) = h_o + h_1 z + h_2 z^2 + \ldots$, where

$$h_o = 2r_o^2 \cdot \left[\frac{\alpha'(r_o)}{r_o} + U(r_o) - k^2 + \frac{1}{4}\,\alpha''(r_o)\right] \quad , \text{ etc.} \tag{C12}$$

Then

$$I(\Delta r) = \frac{1}{g} \int_{-\Delta r}^{+\Delta r} \left(\frac{1}{z} - \frac{h(z)}{g + z\, h(z)}\right) dz = I_1 + I_2(\Delta r) \quad . \tag{C13}$$

The second integral, $I_2(\Delta r)$, is a dull, well behaved function of Δr. To lowest order in r it is

$$I_2(\Delta r) \simeq - \frac{2 h_o}{g^2} \Delta r + \mathcal{O}((\Delta r)^3) \quad . \tag{C14}$$

To evaluate I_1 however, we must detour around the pole in the integrand. For a continuation of the solution when the pole is above the axis ($c_2 < 0$), we use the z-plane contour

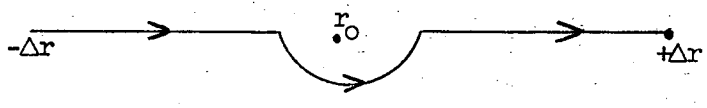

Then $I_1 = +i\pi/g$. Similarly, for a continuation of the solution when $c_2 > 0$, we must go above the pole. This yields $I_1 = -i\pi/g$. Substituting all this back into Eq. (C9), and expanding everything to lowest order in Δr, we have

$$X(r_2) = X(r_1) \pm \frac{i\pi}{g} \psi(r_1) + 2\Delta r \left[a_1 (1 \pm i \frac{\pi}{2}) X(r_1) + \frac{h_o}{g} \psi(r_1) \right] + \ldots \tag{C15}$$

$$\psi(r_2) = \psi(r_1) + 2a_1 \Delta r \left[(-1 \pm i \frac{\pi}{2}) \psi(r_1) + g X(r_1) \right] + \ldots \quad ,$$

where the upper sign corresponds to continuation from negative c_2, and

$$a_1 = (U(r_o) - k^2)/\alpha'(r_o) \quad .$$

Thus even if the radial wave function $X(r)$ started off real for

small r, as it could if the optical potentials $(U(r), \alpha(r))$ were real, it would develop an imaginary part on propagation through the singular point r_o. Consequently the logarithmic derivative at the boundary $R > r_o$, defined by

$$\lambda(R) \equiv 1 + \psi(R)/R\chi(R)$$

will be complex even in the limit of a real optical potential. And since the sign of its imaginary part depends on whether c_2 approaches zero from above or below, Im $\lambda(R)$ will have a discontinuity at $c_2 = 0$. If we let $U(r) = b\,\rho(r)$, and consider $\lambda(R)$ as a function of the two complex variables $b = b_1 + ib_2$ and $c = c_1 + ic_2$, we have in general $\lambda(b^*, c^*) = \lambda^*(b,c)$. This implies that when the local potential is complex $(b_2 \neq 0)$, Re $\lambda(R)$ also develops a discontinuity at $c_2 = 0$.

The conclusion is then that the Kisslinger model wave function $\chi(r)$ and its logarithmic derivative $\lambda(R)$ are in general not continuous functions of the interaction parameters b and c, there being in particular a discontinuity in $\lambda(R)$ as $c_2 \equiv$ Im c passes through zero. Since $I_1 = \pm i\,\pi/g$, where $g \equiv r_o^2\alpha'(r_o) = -r_o^2\rho'(r_o)/\rho(r_o)$, this discontinuity depends inversly on the gradient of the nuclear density at the singular point. These wave function branch point effects will evidently be absent in only 3 cases:

(i) If $\alpha(0) = c_1\rho(0) > -1$, there is no singular point near physical values of r.

(ii) If $B = \psi(r_o) = 0$, (Eqs. (C7) and (C8)) the singular component is absent from the physical solution.

(iii) In the limit of a uniform square well nuclear density distribution, $g \to \infty$ and $I_1 \to 0$.

REFERENCES AND FOOTNOTES

* Work done under auspices of the U. S. Atomic Energy Commission

1. M. M. Sternheim and R. Hofstadter, Nuovo Cimento 38, 1854 (1965).
2. E. H. Auerbach, D. M. Fleming and M. M. Sternheim, Phys. Rev. 162, 1683 (1967).
3. K. M. Crowe, A. Fainberg, J. Miller and A. S. L. Parsons, Measurement of $\pi^{\pm}$ - He Scattering and its Relation to the Pion Form Factor, UCRL-18473, Sept. 1968, submitted to Physical Review.
4. M. Ericson, Nuovo Cimento 47, 49 (1967).
5. L. I. Schiff, Suppl. of Progr. Theoret. Phys. (Kyoto) Extra No., 400 (1965).
6. Geoffrey B. West, J. Math. Phys. 8, 942 (1967).
7. Geoffrey B. West, Phys. Rev. 162, 1677 (1967).
8. M. M. Block, Phys. Letters. 25B, 604 (1967).
9. M. M. Block et al., Phys. Rev. 169, 1074 (1968).
10. A. Messiah, Quantum Mechanics, translated by G. M. Temmer, (North Holland Publishing Co., Amsterdam; John Wiley and Sons, Inc. New York 1961) Vol. I, Ch. XI.
11. H. Frank, D. Haas and H. Prange, Phys. Letters 19, 391, 719 (1965); G. R. Burleson and H. W. Kendall, Nucl. Phys. 19, 68 (1960).
12. The error function is defined by $\operatorname{erf}(z) \equiv \frac{2}{\sqrt{\pi}} \int_0^z e^{-x^2} dx \equiv 1 - \operatorname{erfc}(z)$
13. Geoffrey F. Chew, S-Matrix Theory of Strong Interactions, (W. A. Benjamin, Inc., New York, 1961) Ch. 15; Richard Wilson, Physics Today, p. 47, Jan. 1969; S. D. Drell and F. Zachariasen,

Electromagnetic Structure of Nucleons, (Oxford Univ. Press, 1961).

14. Equation (20) was derived using formula no. 26, p. 74 of Vol. 1, Tables of Integral Transforms, California Institute of Technology Batemann manuscript Project, A. Erdélyi, Ed. (McGraw-Hill, New York, 1954).

15. K. M. Watson, Phys. Rev. 105, 1388 (1957); A. L. Fetter and K. M. Watson, The Optical Model, in Advances in Theoretical Physics, K. A. Brueckner, Ed. (Academic Press, New York, 1965), p. 115.

16. L. S. Kisslinger, Phys. Rev. 98, 761 (1955).

17. M. Ericson and T. E. O. Ericson, Ann. Phys. 36, 323 (1966)

18. J. V. Lepore and R. J. Riddell (Lawrence Radiation Laboratory) private communication.

19. J. Rix and R. M. Thaler, Phys. Rev. 152, 1357 (1966).

20. I would like to thank Dr. Alfred Goldhaber for this suggestion.

21. G. Cocho and Harun Ar-Rashid, Progr. Theoret. Phys. 36, 1150 (1966).

22. "Asymptotic" is used here to means "In regions where $V \to 0$". Typically, this is for $r \to \infty$.

23. Marvin L. Goldberger and Kenneth M. Watson, Collision Theory, (John Wiley and Sons, Inc., New York, 1964), p. 340 .

24. E. T. Whittaker and G. N. Watson, A Course of Modern Analysis, (Cambridge University Press, 1962), Ch X .

Table I. Model independent fit parameters for S,P, and D waves

p_{Lab} (MeV/c)	ℓ	Logarithmic derivative avg. and diff. (S_ℓ, D_ℓ)				Nuclear phase shifts $\delta_\ell^{\pm}$ (degrees)**			
		Re S_ℓ	Im S_ℓ	Re D_ℓ	Im D_ℓ	Re δ_ℓ^+	Im δ_ℓ^+	Re δ_ℓ^-	Im δ_ℓ^-
130.2	S	-1.161±0.007	-0.110±0.008	4.18±0.21	0.40±0.24	-7.3±0.2	2.2±0.2	-9.0±0.2	2.3±0.2
142.3	S	-1.928±0.008	-0.125±0.008	6.07±0.18	0.89±0.19	-7.7±0.1	1.6±0.2	-9.5±0.1	2.0±0.1
153.2	S	-2.931±0.021	-0.172±0.021	9.90±0.74	1.45±0.74	-8.2±0.3	1.5±0.3	-9.7±0.3	1.8±0.3
163.0	S	-4.304±0.034	-0.326±0.033	14.67±0.86	2.83±0.88	-8.3±0.3	1.8±0.3	-10.1±0.2	2.1±0.2
130.2	P	0.520±0.004	-0.067*±0.005	1.61±0.12	0.13*±0.16	8.7±0.1	1.8±0.2	8.9±0.1	1.9±0.2
142.3	P	0.174±0.004	-0.100*±0.005	2.05±0.07	0.17*±0.11	10.9±0.1	2.6±0.1	11.1±0.1	2.8±0.1
153.2	P	-0.191±0.007	-0.154*±0.009	2.24±0.22	0.30*±0.32	12.8±0.2	3.8±0.3	12.6±0.2	4.0±0.3
163.0	P	-0.611±0.007	-0.226*±0.010	2.80±0.18	0.55*±0.28	14.9±0.2	5.0±0.3	14.7±0.2	5.3±0.3
130.2	D	2.100±0.009	-0.013*±0.012	0.70±0.29	0.02*±0.36	1.0±0.1	0.1±0.1	1.0±0.1	0.1±0.1
142.3	D	1.921±0.006	-0.015*±0.007	0.78±0.12	0.02*±0.16	1.5±0.1	0.1±0.1	1.5±0.1	0.2±0.1
153.2	D	1.750±0.009	-0.020*±0.010	$0.88^{*}{}^{+0.30}_{-0.90}$	0.03*±0.25	2.0±0.1	0.2±0.2	2.0±0.1	0.3±0.2
163.0	D	1.568±0.007	-0.022*±0.008	1.00±0.18	0.04*±0.20	2.7±0.1	0.3±0.1	2.7±0.1	0.3±0.1

*These variables arbitrarily fixed at "reasonable values" in final fit (see text).

**Listed errors on (S_ℓ, D_ℓ) are the deviations that increase χ^2 by 10%. They are propagated crudely to the phase shifts using Eqs. (25) and (26).

Table II. Kinematics and fit guality

data set	p_{Lab} (MeV/c)	k (F^{-1})	η	CM kinetic energy (MeV) T_π	T_α	irms error $\bar{p}$	$\sigma_\pm(\theta)$ fits 30 data pts. χ_+^2	χ_-^2	χ_σ^2	$\Delta(\theta)$ fits 15 data pts. $\overline{\delta\Delta}$	χ_Δ^2
a	130.2	0.6280	.0209	47.1	2.1	.045	21.1	16.3	37.4	.063	14.9
b	142.3	0.6850	.0199	54.7	2.4	.022	71.1	40.5	111.6	.022	29.2
c	153.2	0.7361	.0192	61.8	2.8	.042	37.2	17.4	54.6	.054	21.9
d	163.0	0.7818	.0186	68.4	3.2	.028	55.2	35.2	90.4	.033	28.0

UCRL-19216

Table III. Modified Kisslinger model optical parameters

data set*	fake ImS_1	c (F^3)	readjusted local const. b(F) S wave	P wave	D wave
a	-0.13	-6.40-0.16 i	1.24-0.26 i	1.16+0.41 i	3.15+0.22 i
b	-0.19	-6.62-0.25 i	1.37-0.15 i	1.87+0.59 i	3.42+0.59 i
b'	-0.19	-6.14-0.10 i	1.28-0.17 i	1.82+0.61 i	2.27+0.66 i
c	-0.25	-6.61-0.26 i	1.50-0.07 i	1.98+0.53 i	3.79+0.47 i
d	-0.35	-6.78-0.15 i	1.65-0.04 i	2.20+0.50 i	4.10+0.41 i

*Model b' has density radius parameter a_N = 1.27 F. (cf. Eq. (52)).

The rest have a_N = 1.34 F.

Table IV. Local model optical parameters (c = 0)

data set	adjusted b(F) S wave	P wave	D wave
a	1.08 - 0.34 i	-6.47 - 0.92	-12.31 - 0.90 i
b	1.10 - 0.26 i	-6.59 - 1.10	-12.70 - 0.92 i
b'	1.07 - 0.26 i	-6.78 - 1.08	-14.30 - 0.99 i
c	1.12 - 0.23 i	-6.58 - 1.36	-12.39 - 1.12 i
d	1.13 - 0.27 i	-6.75 - 1.56	-12.67 - 1.10 i

Table V. Pion radii from minimizing χ_Δ^2 for various models

pion model data set	Modified Kisslinger nuclear model					ℓ dependent local potential nuclear model				
	Gaussian			Yukawa		Gaussian			Yukawa	
	r_π*	Δr_π	χ_Δ^2	r_π	Δr_π	χ_Δ^2	r_π	Δr_π	χ_Δ^2	r_π	Δr_π	χ_Δ^2
a	2.64	± .39	19.9	3.02	± .51	19.2	2.26	± .41	19.0	2.52	± .51	18.4
b	2.70	± .23	58.2	3.12	± .30	52.0	2.19	± .29	71.5	2.44	± .35	66.0
b'	2.63	± .25	64.9	3.02	± .32	57.8	2.21	± .30	77.9	2.47	± .37	71.8
c	3.03	± .61	49.6	3.61	± .82	46.3	2.35	± .72	53.6	2.71	± .89	50.7
d	3.32	± .42	51.9	4.02	± .57	47.7	2.63	± .50	60.6	3.05	± .64	56.0

*All radii in fermis

UCRL-19216

FIGURE CAPTIONS

Fig. 1. Nuclear density distribution $\rho(r)/\rho(0)$, and effective coulomb potentials $V_C(r)$ (MeV) for Gaussian pion charge distribution (Eq. (18)) with r_π = 0,1,2, and 3 F.; Yukawa pion charge distribution (Eq. (20)) with r_π = 2 F. (dashed curve); and pure $1/r$ potential of two point charges (curve P).

Fig. 2. Total absorbtion cross sections (mb) vs. lab momentum (MeV/c) for π^+ (triangles) and π^- (circles). Solid symbols are data from Ref. 9, open symbols are calculated values from fit parameters of Table I.

Fig. 3. Elastic differential cross sections $\sigma^{\pm}(\theta)$ (mb/sr) vs. $\cos\theta_{CM}$ for $\pi^{\pm}$ on He^4. Theoretical curves are calculated from the model independent fit parameters of Table I. Triangles are π^+ data; circles are π^- data.

Fig. 4. Fractional difference data $\Delta(\theta)$ vs. $\cos\theta_{CM}$. Curve MI calculated from model independent fit parameters of Table I; Curve for $r_\pi = 0$ calculated using Kisslinger model wave functions in Eq. (35).

Fig. 5. Real part of normalized weighting functions $Y_\ell^2(r) = \left[r\,\chi_\ell^o(r)/\,R\chi_\ell^o(R)\right]^2$ for S,P, and D waves at 142.3 MeV/c lab momentum. Solid curves for modified Kisslinger model, dashed curves for local potential model.

Fig. 6. Re D_ℓ vs. $r_\pi(F)$ for S,P, and D waves at 142.3 MeV/c (data set b). Horizontal bands are data values and errors from model independent fit (Table I). Solid curves (G) calculated from Eq. (35) with Gaussian pion charge distribution using wave functions generated by local (L) and Kisslinger (K) nuclear interaction models. Curves for free particle wave functions (F) are shown for comparison. Dashed curves (Y) are for Yukawa pion model (Eq. (20)). The "data points" are the fitted pion radii and errors from Table V.

Fig. 7. χ_Δ^2 vs. $r_\pi(F)$ for Gaussian pion model and both nuclear models. Labels a,b,c,d refer to the data sets at the four beam momenta (cf. Table II).

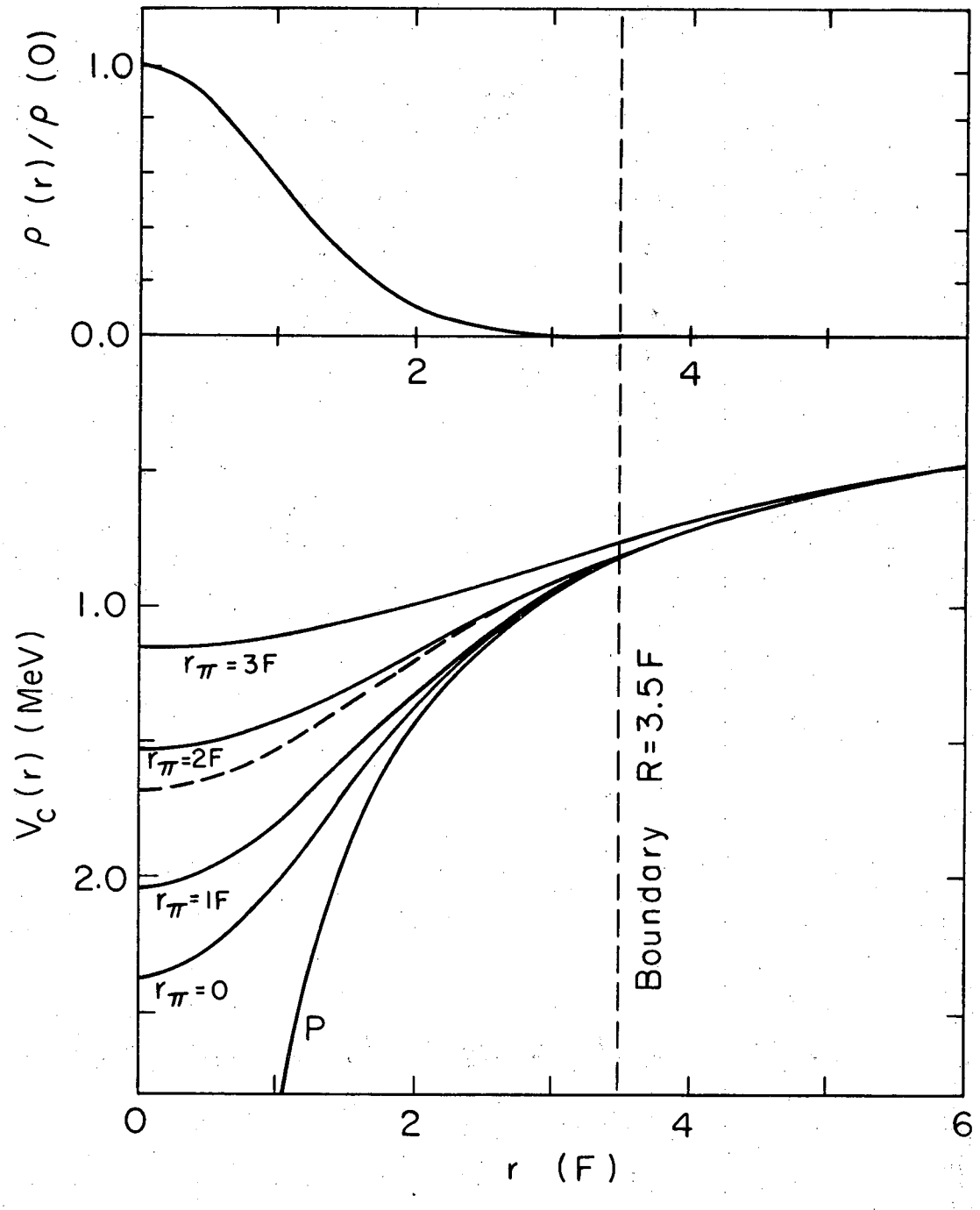
ρ (r) / ρ (0)
1.0
0.0
2
4
1.0
2.0
V_c (r) (MeV)
r_π = 3F
r_π=2F
r_π=1F
r_π = 0
P
Boundary R=3.5F
0
2
4
6
r (F)
XBL 696-3122

Fig. 1.

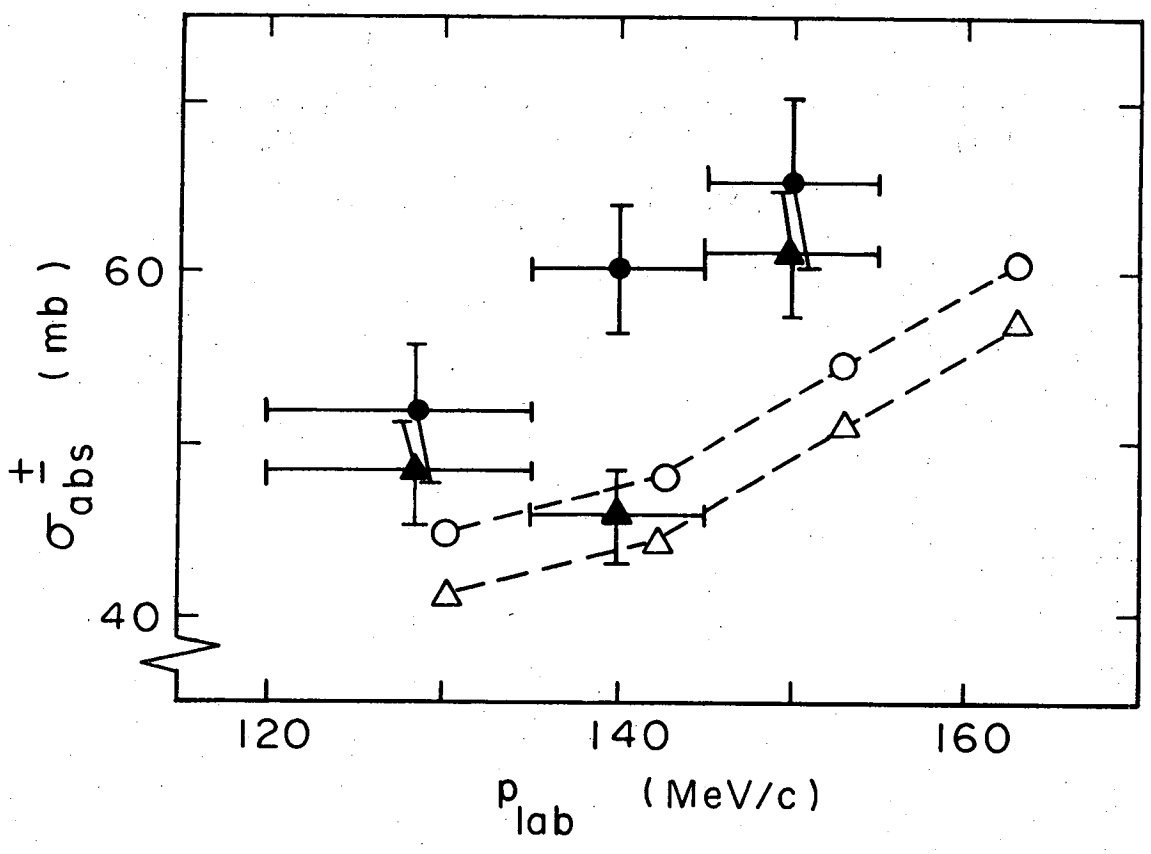

XBL696-3123

Fig. 2.

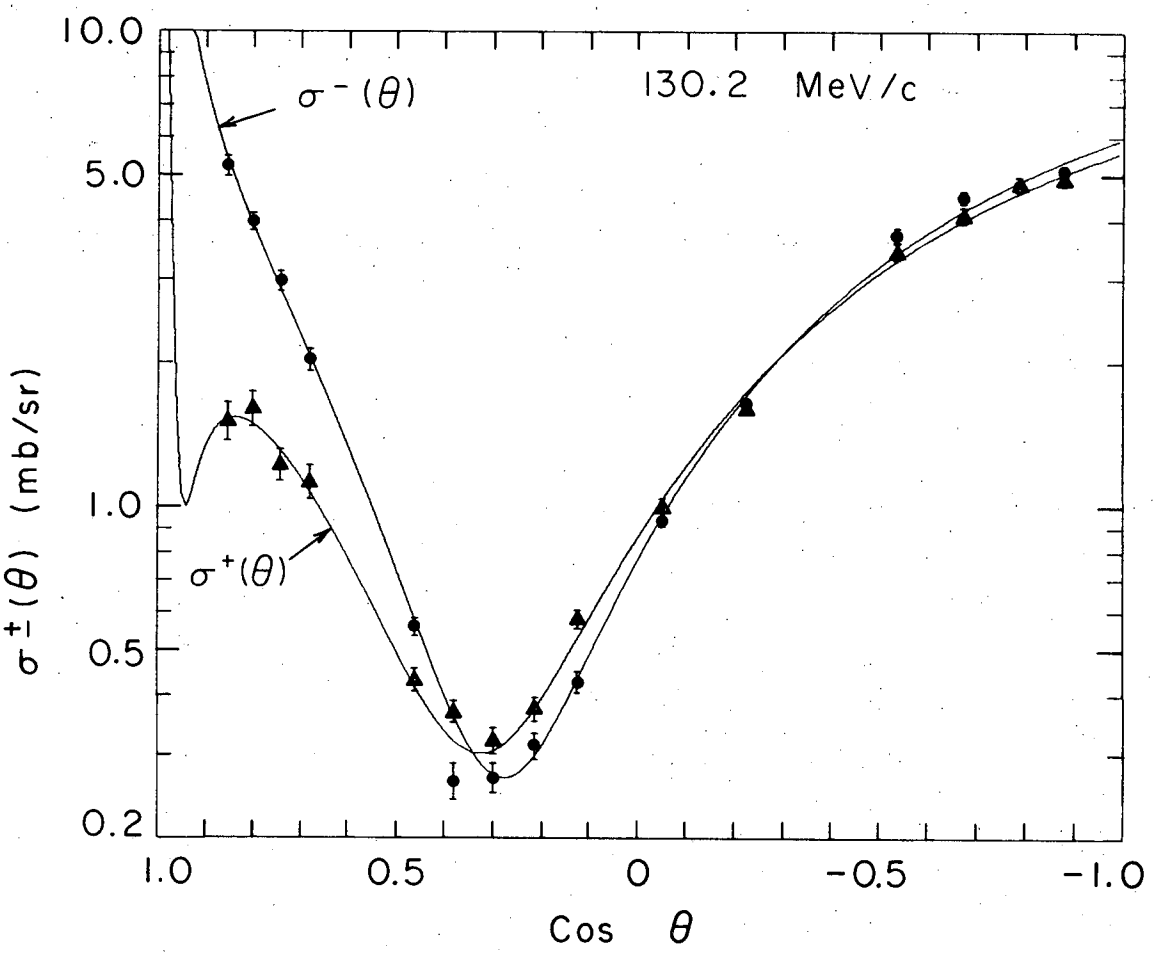

XBL696-3132

Fig. 3a.

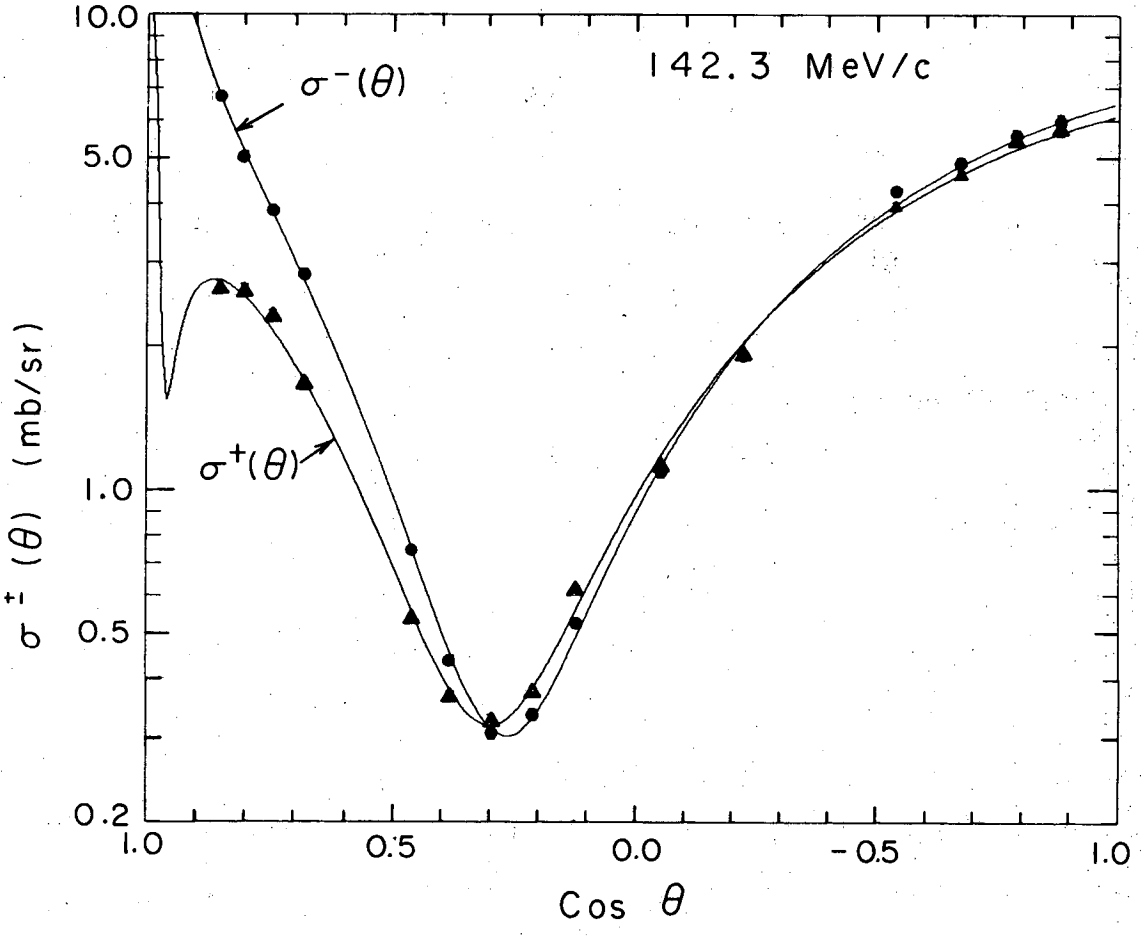

XBL696-3133

Fig. 3b.

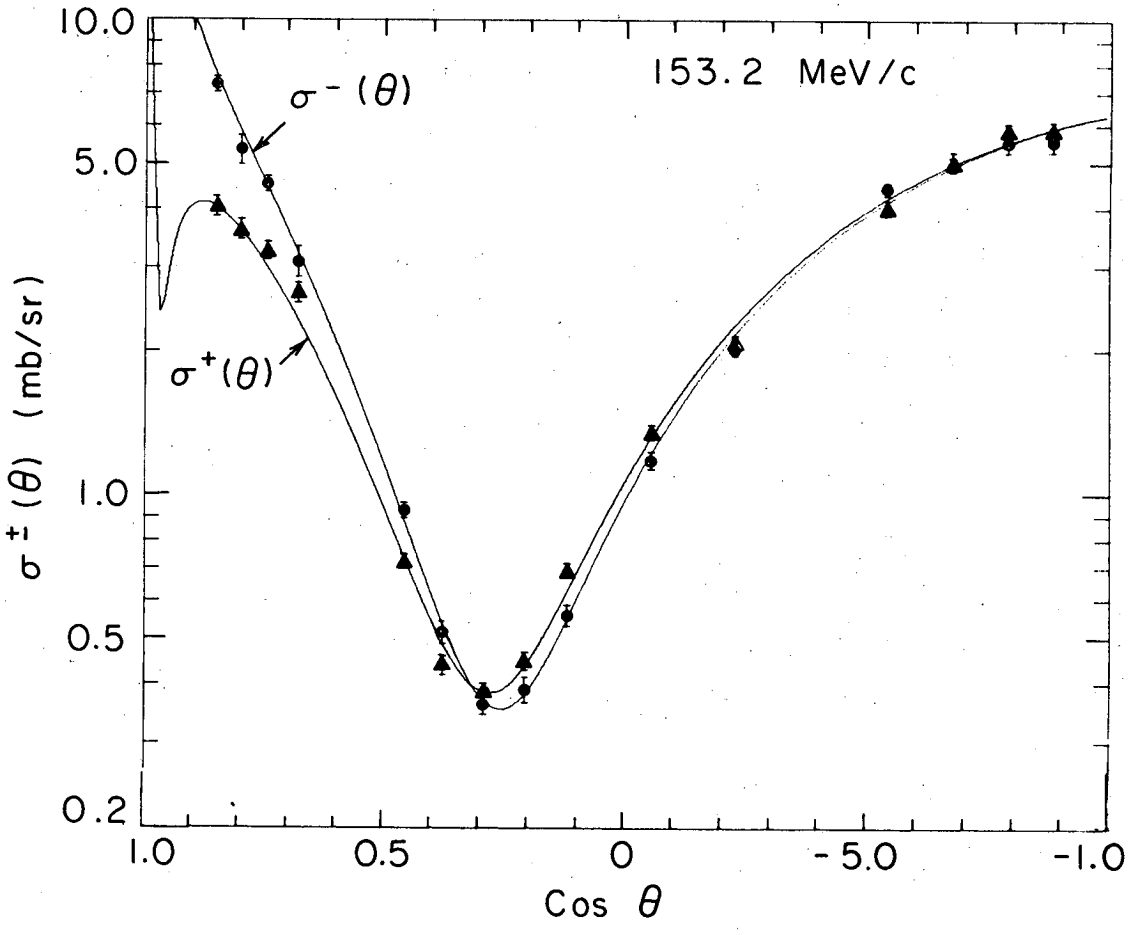

XBL696-3134

Fig. 3c.

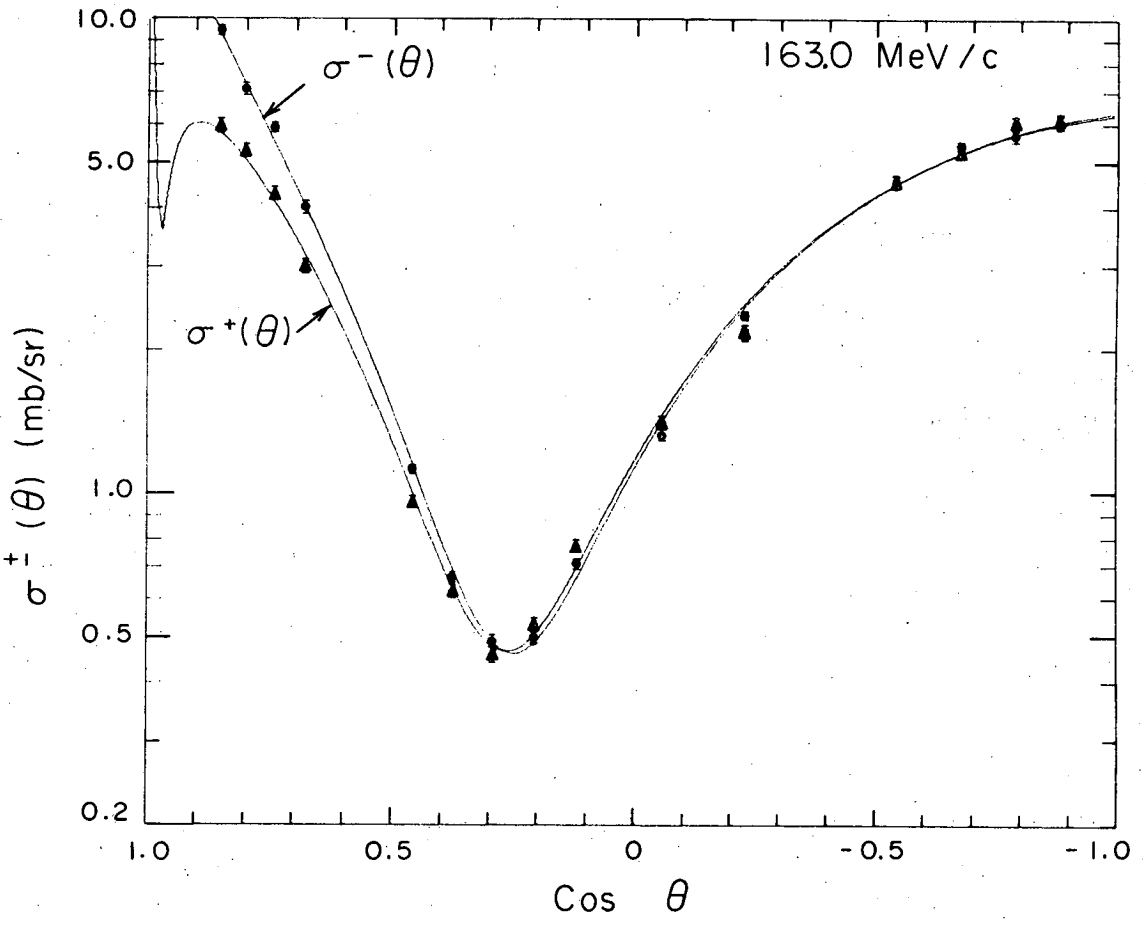
10.0
5.0
1.0
0.5
0.2
1.0
0.5
0
-0.5
-1.0
Cos θ
σ± (θ) (mb/sr)
σ⁻(θ)
σ⁺(θ)
163.0 MeV/c
XBL696-3135

Fig. 3d.

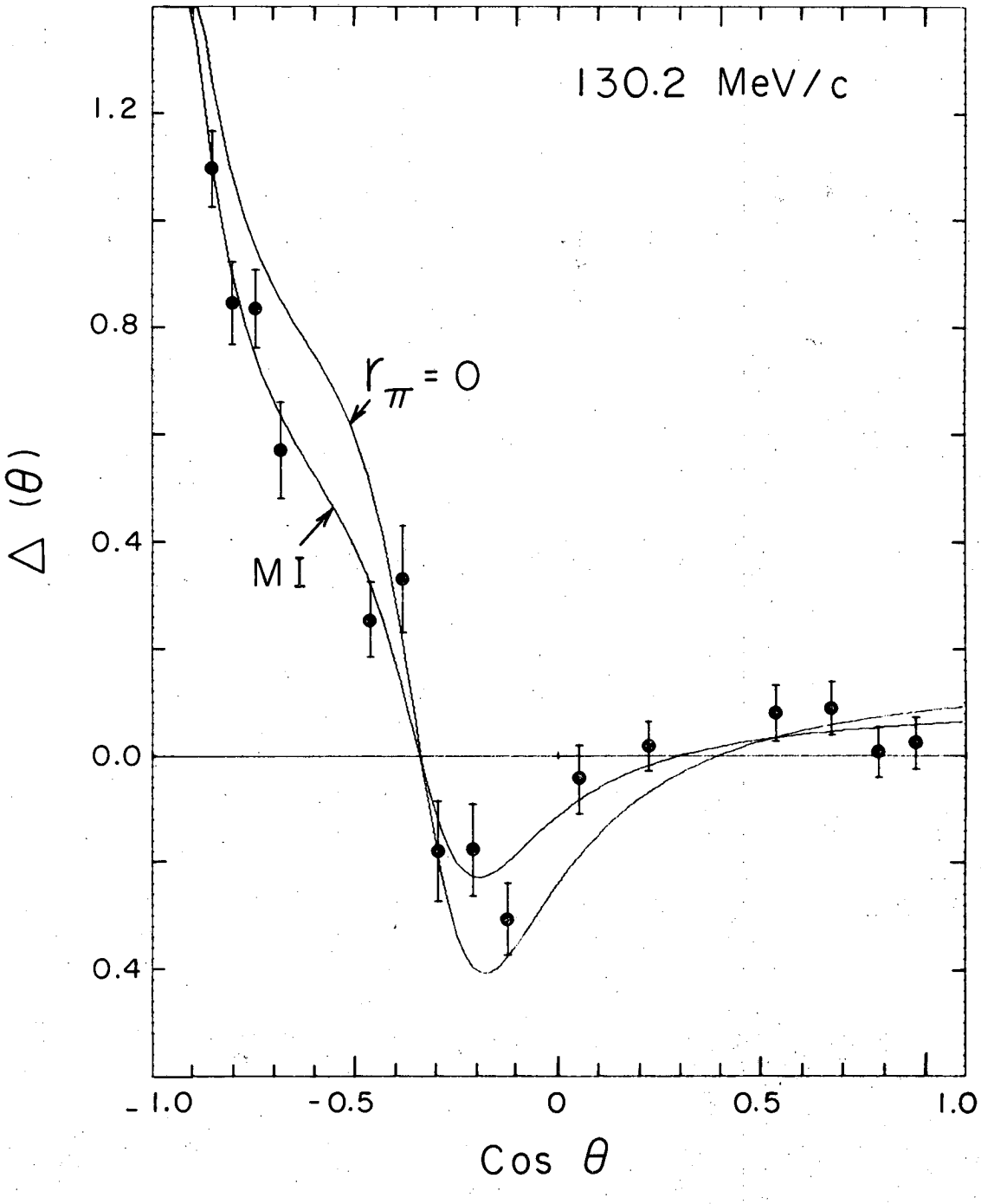

Fig. 4a.

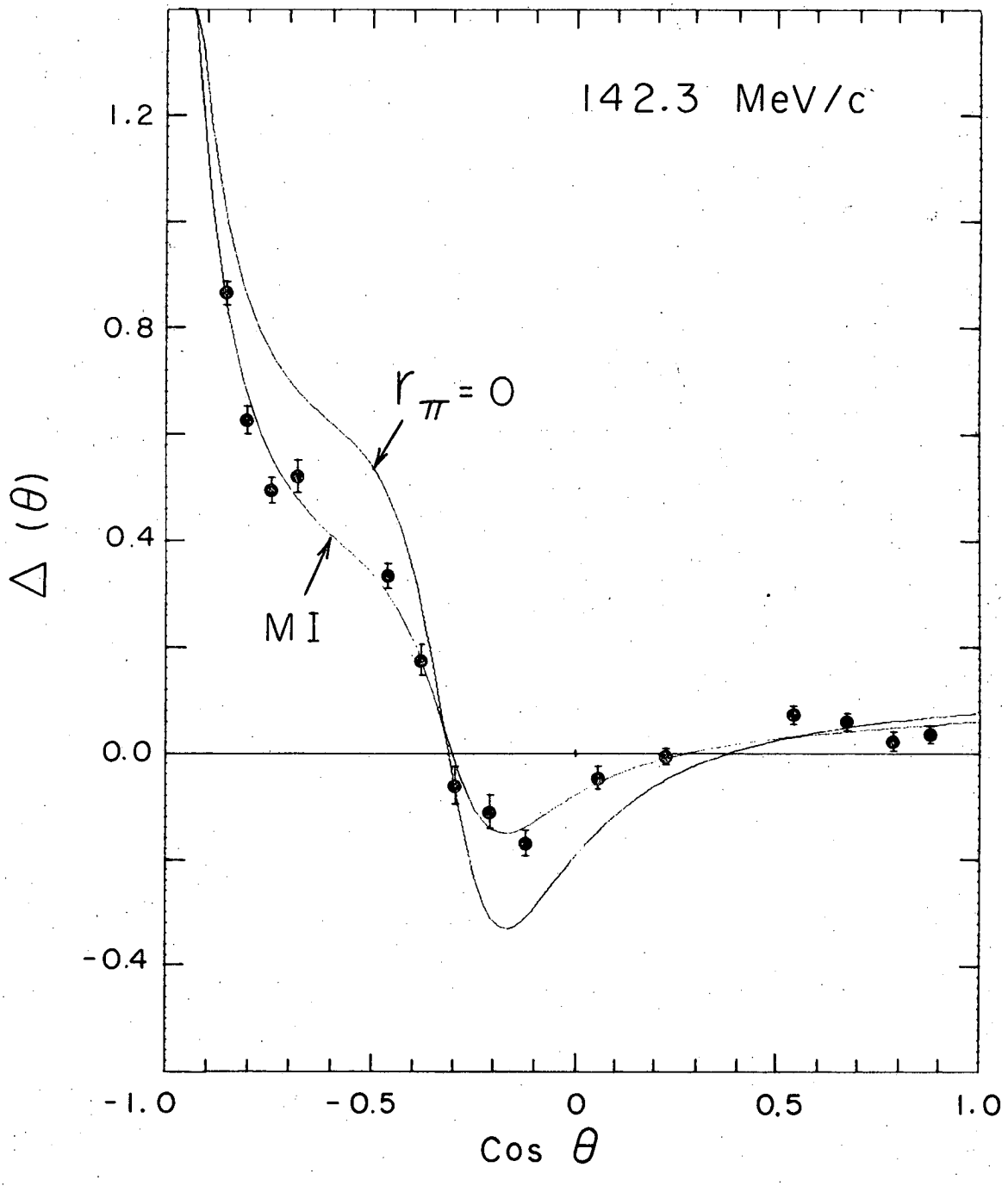

Fig. 4b.

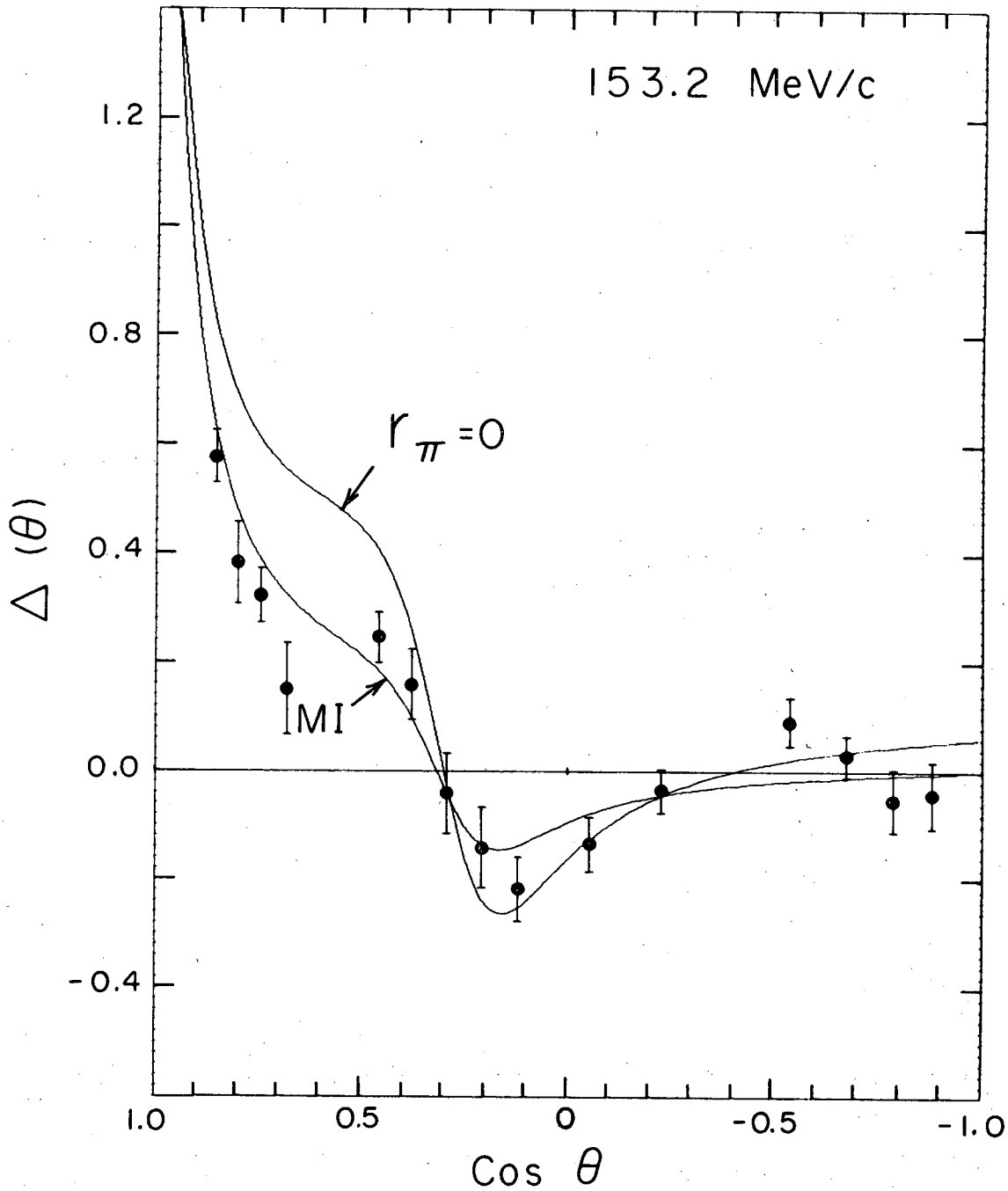

XBL696-3130

Fig. 4c.

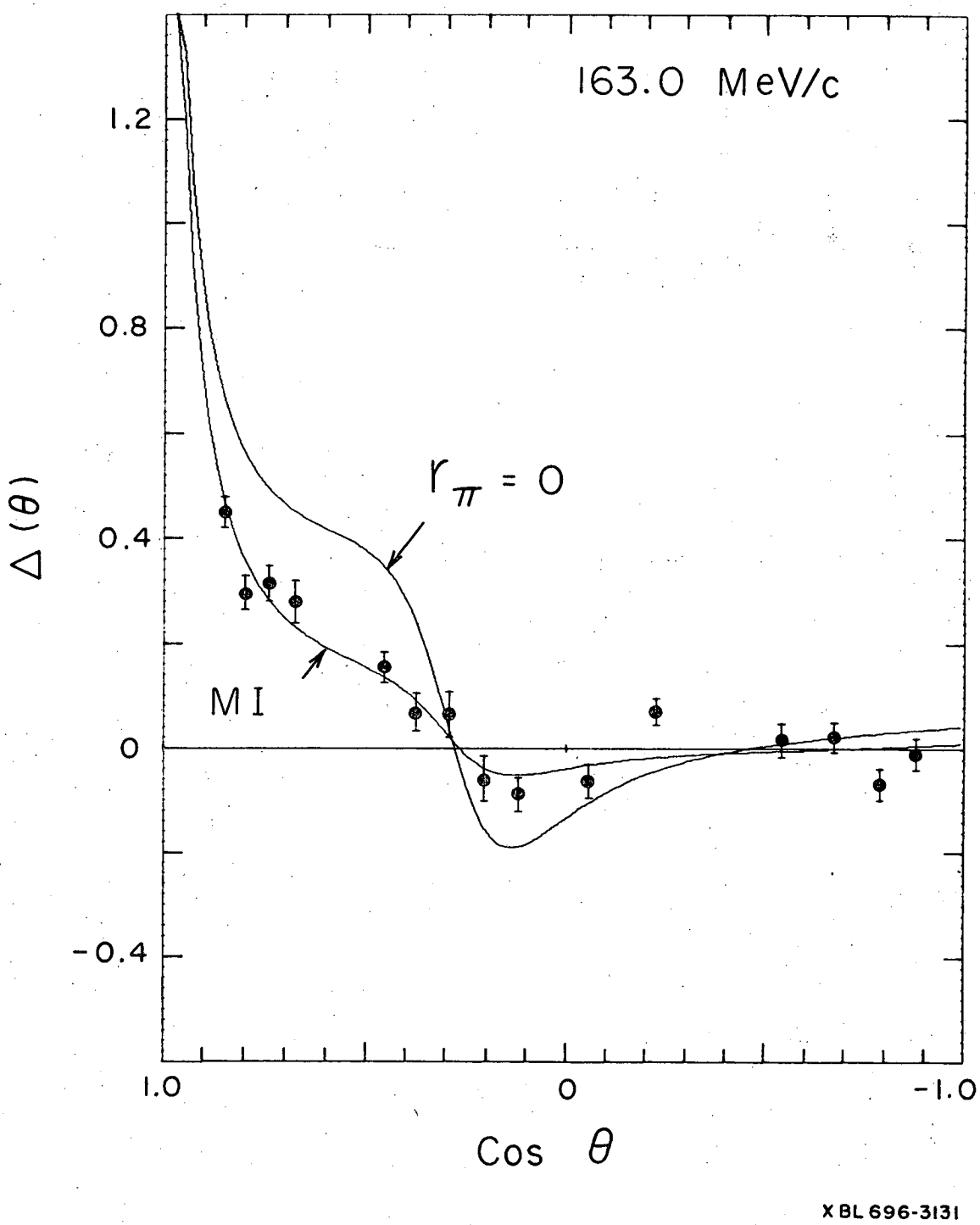

Fig. 4d.

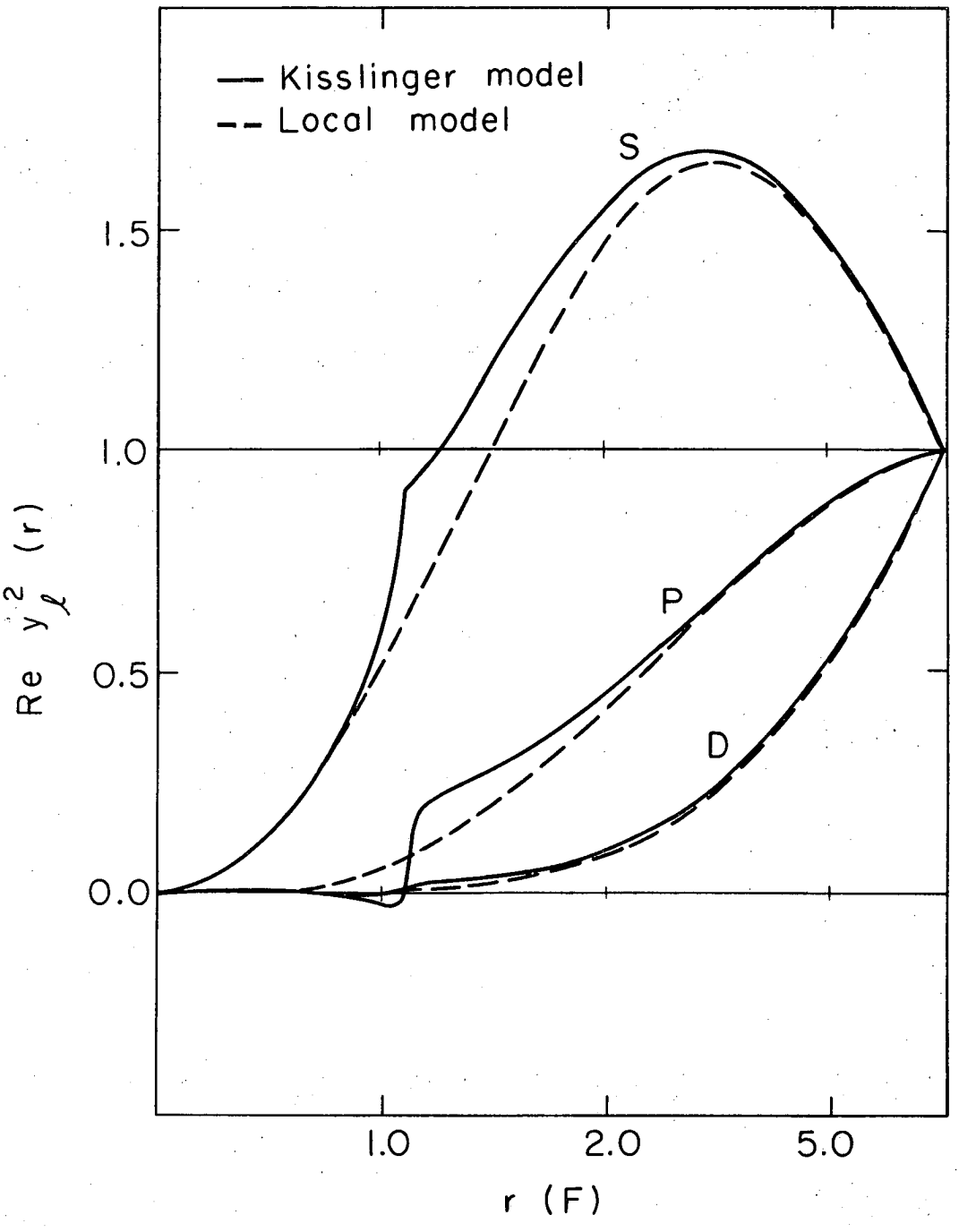
Kisslinger model
Local model
S
P
D
1.5
1.0
0.5
0.0
Re y_ℓ^2 (r)
1.0
2.0
5.0
r (F)
XBL696-3124

Fig. 5.

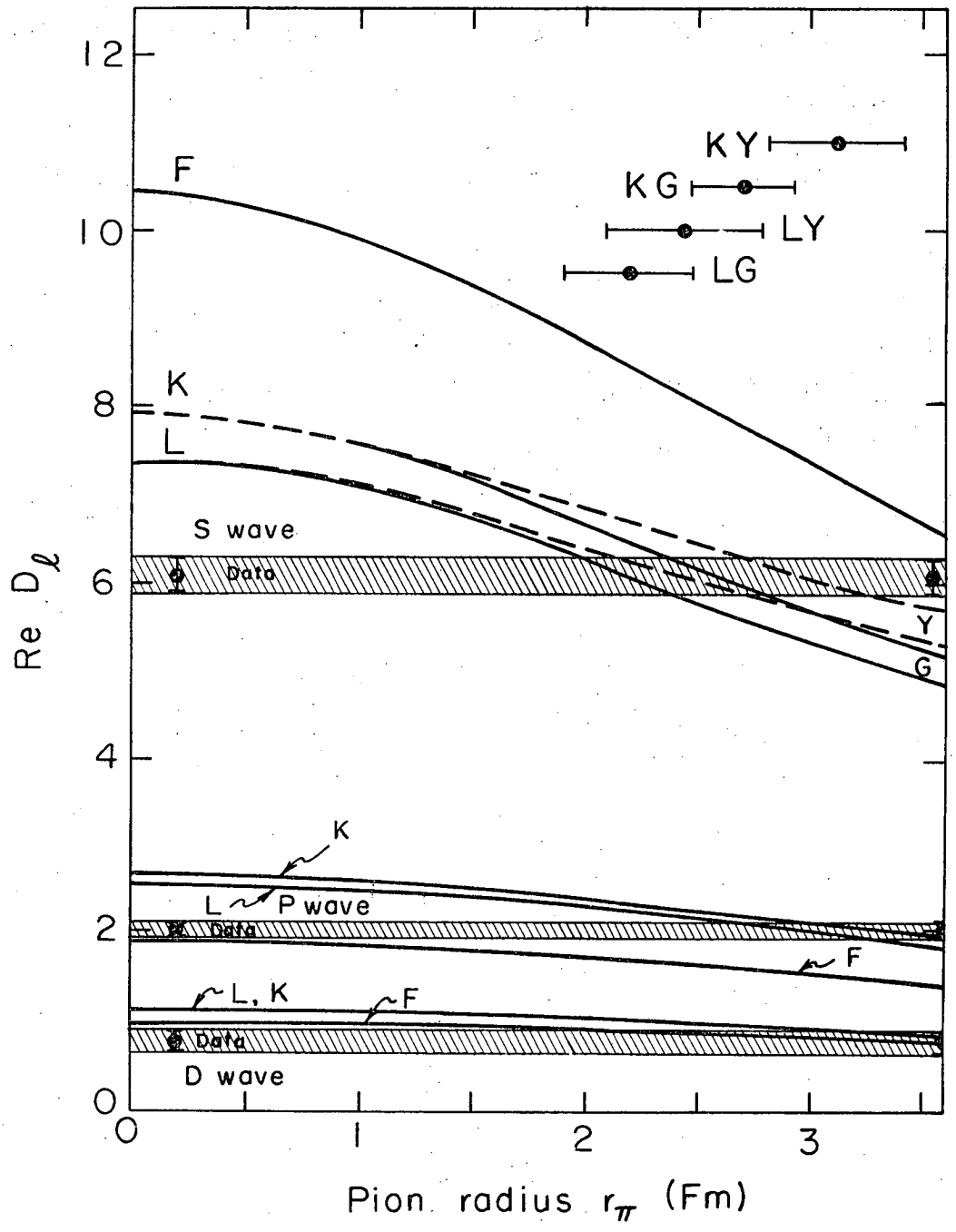
12
10
8
6
4
2
0
Re D_ℓ
F
K
L
S wave
Data
Y
G
K Y
K G
L Y
L G
K
L
P wave
Data
F
L, K
F
Data
D wave
0
1
2
3
Pion radius r_π (Fm)
XBL696-3125

Fig. 6.

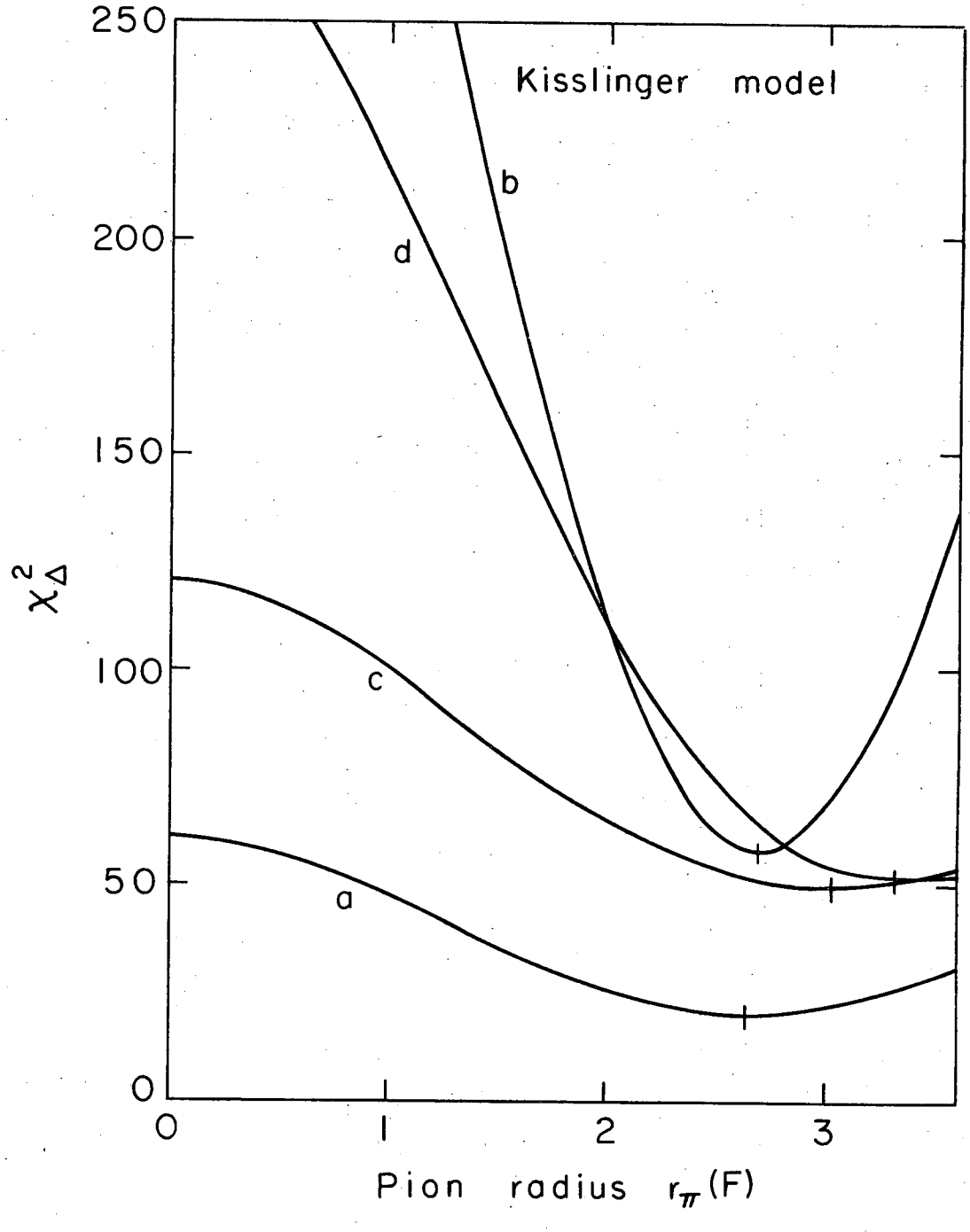

XBL696-3126

Fig. 7a.

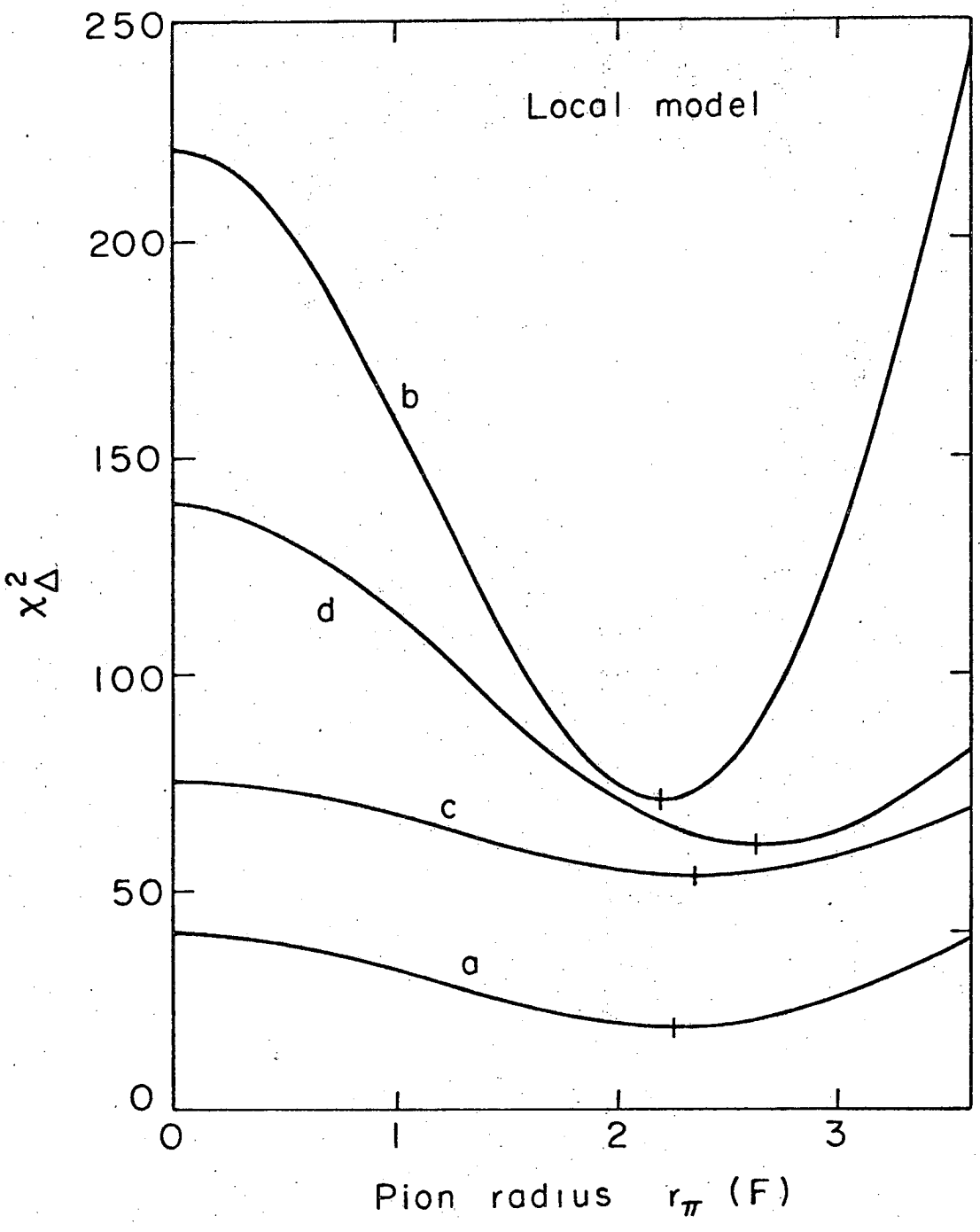

XBL696-3127

Fig. 7b.

TECHNICAL INFORMATION DIVISION
LAWRENCE RADIATION LABORATORY
UNIVERSITY OF CALIFORNIA
BERKELEY, CALIFORNIA 94720